Master Thesis

A Variable Gain Physiological Controller for Rotary Ventricular Assist Devices

by **Luís Felipe Vieira Silva**

advised by
Prof. Ph.D. Thiago Damasceno Cordeiro

Federal University of Alagoas
Computing Institute
Maceió, Alagoas
February 11, 2022

Catalogação na Fonte
Universidade Federal de Alagoas
Biblioteca Central
Divisão de Tratamento Técnico

Bibliotecário: Marcelino de Carvalho Freitas Neto – CRB-4 - 1767

S586v Silva, Luís Felipe Vieira.
A variable gain physiological controller for rotary ventricular assistent devices / Luís Felipe Vieira Silva. – 2022.
44 f. : il.

Orientador: Thiago Damasceno Cordeiro.
Dissertação (mestrado em Informática) - Universidade Federal de Alagoas. Instituto de Computação. Maceió, 2022.

Bibliografia: f. 42-44.

1. Coração auxiliar. 2. Controladores fisiológicos. 3. Sistema cardiovascular. I. Título.

CDU: 004.358:612.1

UNIVERSIDADE FEDERAL DE ALAGOAS/UFAL
Programa de Pós-Graduação em Informática – PPGI
Instituto de Computação/UFAL
Campus A. C. Simões BR 104-Norte Km 14 BL 12 Tabuleiro do Martins
Maceió/AL - Brasil CEP: 57.072-970 | Telefone: (082) 3214-1401

Folha de Aprovação

LUIS FELIPE VIEIRA SILVA

UM CONTROLADOR FISIOLÓGICO DE GANHO VARIÁVEL PARA DISPOSITIVOS DE ASSISTÊNCIA VENTRICULAR

Dissertação submetida ao corpo docente do Programa de Pós-Graduação em Informática da Universidade Federal de Alagoas e aprovada em 11 de fevereiro de 2022.

Banca Examinadora:

gov.br Documento assinado digitalmente
Thiago Damasceno Cordeiro
Data: 11/02/2022 21:46:43-0300
Verifique em https://verificador.iti.br

Prof. Dr. THIAGO DAMASCENO CORDEIRO
UFAL – Instituto de Computação
Orientador

gov.br Documento assinado digitalmente
Icaro Bezerra Queiroz de Araujo
Data: 14/02/2022 09:24:19-0300
Verifique em https://verificador.iti.br

Prof. Dr. ICARO BEZERRA QUEIROZ DE ARAUJO
UFAL – Instituto de Computação
Examinador Interno

gov.br Documento assinado digitalmente
Antonio Marcus Nogueira Lima
Data: 12/02/2022 09:18:08-0300
Verifique em https://verificador.iti.br

Prof. Dr. ANTONIO MARCUS NOGUEIRA LIMA
UFCG – Universidade Federal de Campina Grande
Examinador Externo

FEDERAL UNIVERSITY OF ALAGOAS
Computing Institute

A VARIABLE GAIN PHYSIOLOGICAL CONTROLLER FOR ROTARY VENTRICULAR ASSIST DEVICES

Master Thesis submited to the Computing Institute fom Federal University of Alagoas as a partial requirement to obtain the degree in Master in Informatics.

Aproved in February 11, 2022:

Thiago Damasceno Cordeiro,
Prof. Ph.D., Advisor

Antonio Marcus Nogueira Lima,
Prof. Ph.D., UFCG

Ícaro Bezerra Queiroz de Araújo,
Prof. Ph.D., UFAL

Where there is a will, there is a way. After all, miracles happen every day, do they not?
Final Fantasy XIV

Resumo

Este trabalho envolve o projeto de uma lei de controle fisiológico adaptativo para um dispositivo de assistência ventricular turbodinâmico (TVAD) usando um modelo variante no tempo de parâmetros concentrados que descreve o sistema cardiovascular. O TVAD é uma bomba de sangue rotativa acionada por um motor elétrico. A simulação do sistema também inclui o controlador de realimentação adaptativo, que fornece uma saída cardíaca fisiologicamente correta sob diferentes condições de pré-carga e pós-carga. A saída cardíaca é estimada a cada batimento cardíaco e o objetivo de controle é alcançado alterando dinamicamente a referência do controlador de velocidade do motor com base no erro da pressão sistólica. TVADs fornecem suporte para a circulação sanguínea em pacientes com insuficiência cardíaca. Diversas estratégias de controle foram desenvolvidas ao longo dos anos, com destaque para as fisiológicas, que adaptam seus parâmetros para melhorar a condição do paciente. Neste trabalho, uma nova estratégia é proposta utilizando um controlador fisiológico de ganho variável para manter a saída cardíaca em um valor de referência sob alterações tanto na pré-carga quanto na pós-carga. Um modelo computacional é usado para avaliar o desempenho desta técnica de controle, que tem apresentado melhores resultados de adaptabilidade do que controladores de velocidade constante e controladores de ganho constante.

***Palavras-chave*: *Dispositivos de Assistência Ventricular*; *Controladores Fisiológicos*; *Sistema Cardiovascular*.**

Abstract

This work involves designing a physiological adaptive control law for a turbodynamic ventricular assist device (TVAD) using a lumped parameter time-varying model that describes the cardiovascular system. The TVAD is a rotary blood pump driven by an electrical motor. The system simulation also includes the adaptive feedback controller, which provides a physiologically correct cardiac output under different preload and afterload conditions. The cardiac output is estimated at each heartbeat, and the control objective is achieved by dynamically changing the motor speed controller's reference based on the systolic pressure error. TVADs provide support for blood circulation in patients with heart failure. Several control strategies have been developed over the years, emphasizing the physiological ones, which adapt their parameters to improve the patient's condition. In this work, a new strategy is proposed using a variable gain physiological controller to keep the cardiac output in a reference value under changes in both preload and afterload. Computational models are used to evaluate the performance of this control technique, which has shown better adaptability results than constant speed controllers and constant gain controllers.

Keywords*: *Ventricular Assist Devices*; *Physiological Controller*; *Cardiovascular System.

List of Figures

List of Tables

List of Acronyms

CO	Cardiac output
CVS	Cardiovascular System
EDV	End-Diastolic volume
EDP	End-Diastolic pressure
ESPVR	End-systolic pressure-volume relationship
ESV	End-Systolic volume
HCS	Human cardiovascular system
HR	Heart rate
LVAD	Left ventricular assist device
MSE	mean squared error
ODE	Ordinary differential equation
P	Proportional
PI	Proportional integral
PID	Proportional integral derivative
PIP	Pump inlet pressure
PV	Pressure-volume
PVAD	Pulsatile ventricular assist device
RMSE	root mean squared error
RVAD	Rotary ventricular assist device
SP	Systolic pressure
SV	Stroke volume
TVAD	Turbodynamic ventricular assist device
VG	Variable Gain

Contents

Chapter 1

Introduction

Cardiovascular problems such as heart failure are growing at an epidemic rate [Mancini and Colombo, 2015] and heart transplantation remains the primary treatment for terminally ill patients. However, as the number of patients needing heart transplants increases, the number of available organs decreases [Ochsner et al., 2014]. Thus, the use of alternative treatments such as ventricular assist devices (VADs) has become increasingly present [Mancini and Colombo, 2015].

The technology of these devices has gained many improvements over the last 20 years [Daners et al., 2017]. However, these devices need to be safer and more robust for the patient, considering that they can cause thrombosis and bleeding in the user. These events are usually associated with the operating speed of rotary type devices [von Platen et al., 2019]. Therefore, the authors say that the adaptation of devices with a physiological control system is one aspect that needs to be improved in the use of VADs.

The human body can be characterized by a set of variables, some of which are the individual's physical structure, age, and weight, making the adaptability of the functioning of these devices essential. Constant modes of operation provide a good quality of life for a given patient. However, they can present, for example, the phenomenon called suction in other patients, sucking the wall of the ventricles and causing them to collapse. For this reason, physiological controllers applied to VADs, in addition to providing adequate pumping for each patient, have the function of preventing undesirable events [Ochsner et al., 2014].

Physiological control of pumps in LVADs is considered the most efficient way to deal with pumping problems. However, automatic controllers with feedback are not being used in practice [Petukhov et al., 2019][Petrou et al., 2017]. Instead, many algorithms are being used to monitor events such as suction detection and arrhythmia events, among others. It is believed that these adverse events can be detected and prevented by controllers with feedback [Petukhov et al., 2019].

In a review by [AlOmari et al., 2012], a large number of control strategies proposed for VADs were listed, from more classic controllers like P, I, PI, and PID to more modern

ones like adaptive controllers. [Koh et al., 2019], for example, used a predictive control capable of preventing suction while regulating the flow rate of a VAD pump applied to a left ventricle (LVAD). [Wang et al., 2012] developed a feedback controller based on the control current of an LVAD. The simulations in this work show that the controller guarantees the physiological demands of a patient at different levels of activity while avoiding the phenomenon of suction.

Many numerical models representing the entire human cardiovascular system have been used for computational simulation to test such control techniques and algorithms. Models that use electronic components to simulate the circulatory system in a simplified way are called 0D models [Simaan et al., 2008]. The results obtained in the computational simulations need to be tested *in vitro*, for this, hydraulic simulators are set up in the laboratory so that the controller's performance can be tested with real components.

One of the biggest challenges in developing physiological controllers is the selection of feedback signals for the control algorithm. The literature shows results obtained with controllers using estimated flow, blood pressure, or end-diastolic pressure. [Petrou et al., 2016] proposed a controller that uses systolic pressure (SP), called an SP controller, as the main parameter for updating the speed of a rotary VAD. The advantage of this work is to obtain the systolic pressure signal, with the VAD's sensor, without invasive means.

The systolic pressure controller has already been evaluated in the literature ([Malchesky, 2017], [Petrou et al., 2018], [Daners et al., 2017]). However, by updating the pump speed with constant gain, the controller has some limitations. One of the limitations is the inability to adapt to physiological variations such as preload and afterload.

1.1 Problem

A rotary LVAD with the SP controller has the advantage of not requiring invasive means to measure the primary hemodynamic variable that updates pump velocity. However, this controller has limitations; its equation must be calibrated for a specific preload or afterload value; if these values change over time, the controller will need a new calibration due to the constant parameters of the main equation.

In view of this limitation, it's interesting to develop a new algorithm for the SP controller that allows the system to adapt to adverse conditions. As it's known, a patient may suffer physiological changes in clinical environments, e.g., when in a stressful situation or due to cardiac arrhythmia.

The new algorithm for the SP controller needs to undergo the same tests performed on the original controller and new tests with preload and afterload variation to show a possible improvement in the performance when using variable parameters.

A control algorithm for LVADs needs a series of tests and validation steps before being

actually implemented, the first step will be developed in this work with the design and testing *in silico* of the algorithm. The other steps, that can be carried out in future works, are: the implementation *in vitro* of the algorithm in hydraulic simulators; deployment and testing *in vivo* of the algorithm in animals and the last step of validation is made by testing in a small group of humans with LVAD. The last two steps are made with the approval of an ethics committee of internationally recognized research institutions. Each step in the development process of the algorithm depends on the previous step being validated and approved.

1.2 Proposal

The purpose of this work is to present a new adaptable physiological controller for ventricular assist devices that face hemodynamic changes in both preload and afterload.

For this purpose, the SP controller is implemented and simulated using the computational model of the human cardiovascular system developed by Simaan *et al.* [Simaan et al., 2008], with a set of parameters that represents an adult male. A new strategy for this controller is designed to improve its adaptability.

1.3 Structure

This work consists of 6 chapters. Chapter 2 shows the basics of the cardiovascular system, like preload, afterload, cardiac cycle, heart rate, and also presents how the modeling of the human cardiovascular system is made for simulation. Chapter 3 brings the modeling of ventricular assist devices, adds the dynamic model to the pump to get more realistic simulation results, and presents a way to estimate cardiac output when using this type of device. Chapter 4 presents the SP Controller with fixed gain for LVAD and the algorithm of the new proposed controller, the Variable Gain SP Controller. The performance of both controllers is evaluated in experiments using the *root mean squared error* and the *mean squared error* as performance indices. Chapter 5 shows all simulations results of this work and Chapter 6 contains the conclusions and the future works of this work [1].

[1] All the algorithms used in this work can be found at https://github.com/lfelipev/vgsp-controller.

Chapter 2

Modeling the Human Cardiovascular System

This chapter introduces the human cardiovascular system with basic concepts so that the reader can acquire basic knowledge in the area. This chapter also describes the metrics used when analyzing the cardiovascular system, the cardiac cycle is detailed, and the concept of cardiac output, preload, and afterload is also shown.

The chapter also shows how the human cardiovascular system can be modeled for computer simulations through 0D modeling that uses differential equations drawn from electrical circuits.

2.1 The heart structure and the cardiac cycle

The heart can be thought of as two separate pumps, one on the right side that pumps blood through the lungs and one on the left side that pumps blood through the peripheral organs. The ventricles supply the main pumping force that propels blood circulation. The heart has unique mechanisms that cause a continuous succession of contractions, called *heart rhythmicity*, which characterize the heart's rhythmical beat [Hall and Hall, 2020].

The events that happen from the beginning of one beat to the beginning of the next are called the *cardiac cycle*. More specifically, the cycle consists of a period of relaxation called *diastole*, where the heart fills with blood, followed by a period of contraction called *systole*. The duration of the cardiac cycle is the heart rate (HR). For example, if HR is 70 beats/min (bpm), the cardiac cycle duration is 1/70 beats/min or 0.84 seconds per beat.

The events during the cardiac cycle for the left side of the heart can be visualized by the curves shown in Figure 2.2. The three curves at the top show the pressure behavior in the aorta, left ventricle, and left atrium, respectively. The fourth curve shows the changes of volume in the left ventricle and the following two curves are the electrocardiogram and phonocardiogram signal, respectively.

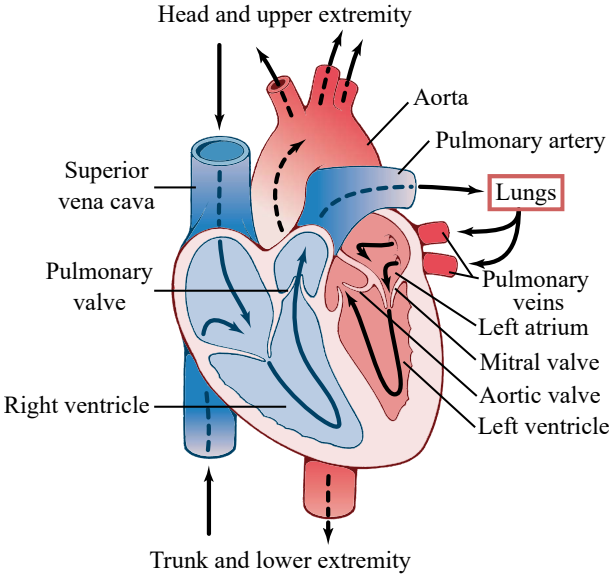

Figure 2.1: Representation of the heart with the course of blood flow through the heart chambers and heart valves. [Hall and Hall, 2020]

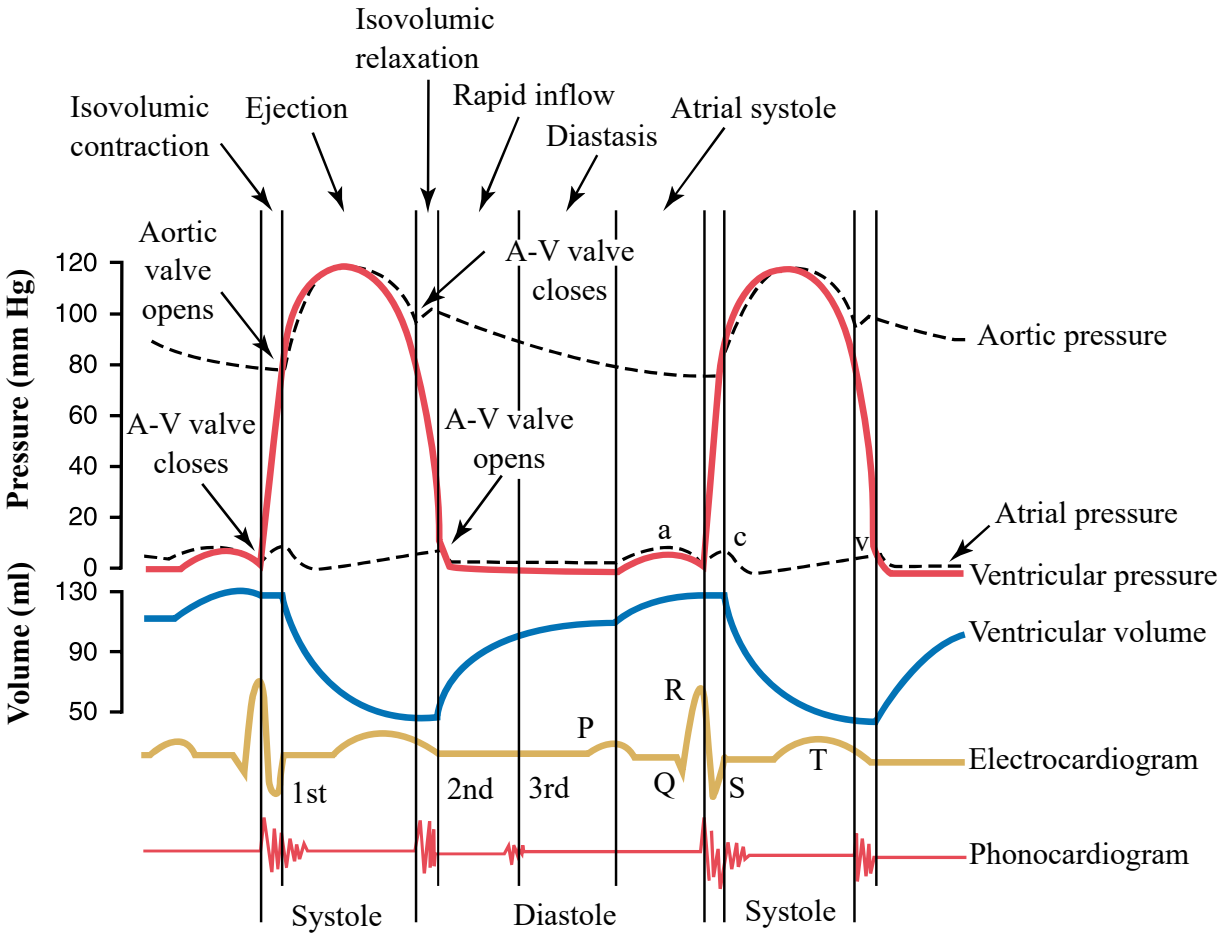

Figure 2.2: Cardiac cycle events for the left ventricle shows left atrial, left ventricular and aortic pressure, the ventricular volume, electrocardiogram, and phonocardiogram. [Hall and Hall, 2020]

The functioning of the ventricles as pumps can be explained using the four stages of the cardiac cycle. The stages are the same for both ventricles. The first stage is the **filling** during diastole, characterized by the large amount of blood accumulated in the atria. At this stage, the growth of the volume curve can be seen in Figure 2.2.

The subsequent stage is the **isovolumic contraction**. At this moment, the volume in the ventricle is kept constant while the heart undergoes an abrupt increase of pressure. When the pressure rises to a certain level, the cycle enters the **ejection** stage, where blood is expelled out of the ventricle.

The last stage before the cycle restarts is the **isovolumic relaxation** allowing the intraventricular pressure to decrease rapidly while the volume is kept constant.

During the stages of the cardiac cycle, some measurements must be taken to obtain relevant information about the cycle: (1) the End-Diastolic Volume (EDV), which is the increase of blood volume in the ventricle during the diastole, (2) the End-Systolic Volume (ESV), which is the remaining volume in the ventricle, and (3) the Stroke Volume (SV), which is the decrease of volume during the systole. The values of these measurements can be used as, for example, heart performance analysis for cardiologists or parameters for controllers, as will be seen in section 4.

2.1.1 Pressure-Volume loop diagram

In the literature, a helpful tool for analyzing left ventricular pumping is the Pressure-Volume (PV) loop diagram, shown in Figure 2.3. The diagram is divided between the four stages of the cardiac cycle. It is possible to obtain information such as the value of EDV, ESV, and SV, or even information about the opening and closing of the heart valves.

Cardiologists can use the PV loop to identify physiological conditions. However, it can also be used as a performance comparator of ventricular assist devices (VAD), devices that can assist cardiac pumping in cases of heart failure.

A large area in the diagram indicates that the heart pumps a large amount of blood, so the ventricle fills with more blood during diastole, extending the diagram to the right. With that, in the contraction stage, the pressure will increase. The extension of the diagram to the left indicates the ejection of blood volume out of the ventricle, then decay of pressure will follow in isovolumetric relaxation.

2.1.2 Cardiac output

The **cardiac output** (CO) can be defined by the amount of blood that the heart transports through the circulatory system in one minute [King and Lowery, 2017]. One way to calculate CO is by measuring the stroke volume (SV). The CO relates the SV and the heart rate (HR) by the following equation:

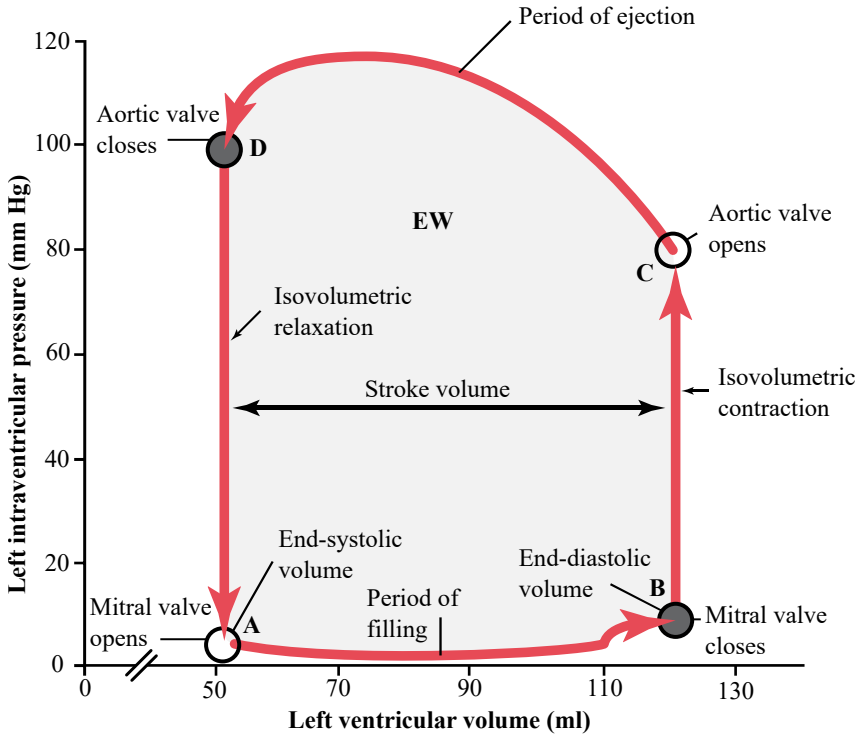

Figure 2.3: Pressure-Volume loop diagram. [Hall and Hall, 2020]

$$CO = SV \times HR \tag{2.1}$$

To calculate the SV, it is necessary to know the end-diastolic volume (EDV) when the ventricle is filled with blood and the end-systolic volume (ESV) when the ventricle ejects it. Therefore the SV can be calculated by the difference in the volume of these two moments as in the following equation:

$$SV = EDV - ESV. \tag{2.2}$$

2.1.3 Preload and Afterload

The degree of tension in the muscle when it starts to contract is called **preload** and is usually considered to be the end-diastolic pressure when the ventricle is filled [Hall and Hall, 2020]. The **afterload** indicates the difficulty that the heart will have to eject the blood, which is directly related to the tension in the muscular wall of the ventricle and uses systolic pressure as an indicator.

Variations in preload and afterload directly affect stroke volume, influencing the cardiac output and the overall heart function. Therefore, understanding preload and afterload are essential to understanding overall cardiac physiology. For example, the abnormal values of these measurements are seen in several conditions, such as heart failure and mitral regurgitation [O'Keefe and Singh, 2020].

2.2 0D Model of the Human Cardiovascular System

The cardiovascular system obeys the laws of mass and momentum conservation, and the blood interaction with the arterial wall can be modeled in different levels of complexity. The most low-level type of modeling, called 0D modeling, uses a coupled system of ordinary differential equations (ODEs) to represent pressure, flow, and blood volume. The 1D models are based on simplified fluid flow equations and can reveal the pressure and flow changes along the whole length of a vessel.

The other higher dimensional models (2D and 3D) are developed with computational fluid dynamics to detail the hemodynamic properties within vessels. These models consider the local vascular geometry derived from reconstructions of medical screening data. Therefore the computational complexity of these models is demanding.

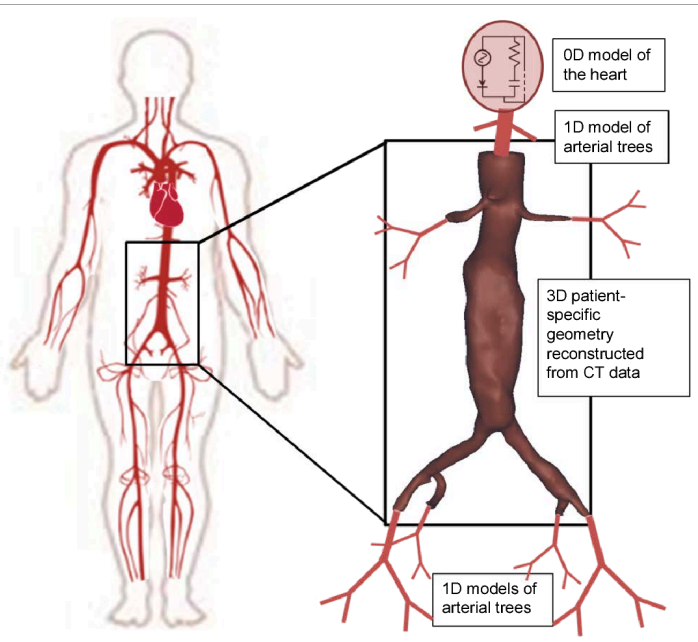

Figure 2.4: The representation of coupling between 0D, 1D and 3D model of the arterial tree [Malatos, 2016].

The 0D model is usually used for control purposes because it demands less computational power than the other models. It is represented with differential equations, thus being represented with mathematical models such as transfer functions and state-space models.

2.2.1 The Windskessel model

Figure 2.5 shows the simplest 0D model of the HCS formulated by [Otto, 1899], the so-called two-element Windkessel model. It consists of a resistor (R) that represents the resistance of the arterial system to the blood flow and a capacitor (C) representing the elasticity of the arteries. With the Windkessel model, the voltage and current in the

circuit are normally calculated using Kirchhoff's laws, with the electric current behaving like the blood flow (Q) in the artery and the voltage behaving like the pressure (P).

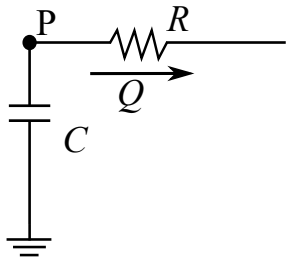

Figure 2.5: The two-element Windkessel model.

In systole, it was shown [Wetterer, 1940] that the two-element Windkessel model poorly predicts the relation between pressure and flow. With Fourier analysis, it was possible to notice the necessity to add an impedance whose modulus, in high frequencies, is equal to the proximal aorta impedance —leading to the creation of the three-element Windkessel model (Figure 2.6).

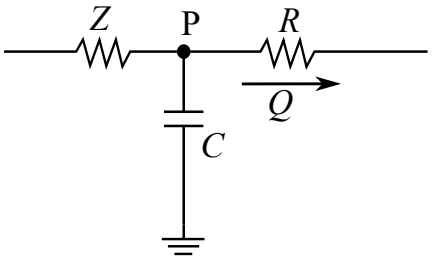

Figure 2.6: The three-element Windkessel model.

To reduce the errors in low frequencies, a fourth element was added to the Windkessel model proposed by [Burattini and Gnudi, 1982]. In this model shown in Figure 2.7, the fourth element consists of an inertance that represents the total inertance of the arterial system.

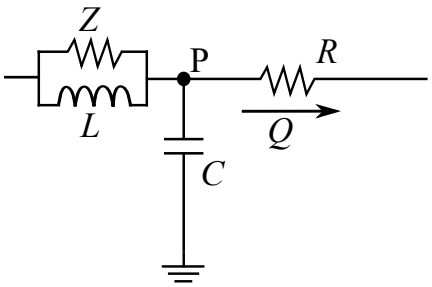

Figure 2.7: The four-element Windkessel model, parallel configuration.

The simplified version of the four-element Windkessel model is shown in Figure 2.8.

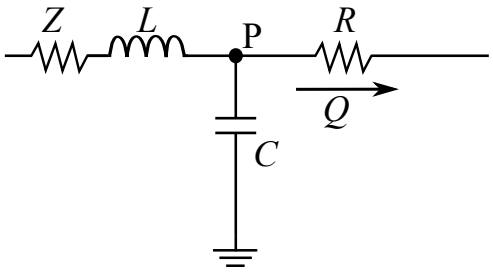

Figure 2.8: The four-element Windkessel model, series configuration.

2.2.2 Ventricle Modeling

As the ventricle works as a reservoir that charges with volume in the filling phase and discharges this volume in the form of blood flow in the ejection phase, in the 0D model, it can be represented by a variable capacitor $C(t)$ (Figure 2.9) where voltage represents volume, and electrical current represents blood flow.

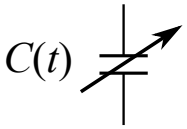

Figure 2.9: A variable capacitor

Capacitance variation needs to be modeled according to a function that represents the behavior of the ventricle. A possible function for this purpose is the elastance function, proposed by [Suga and Sagawa, 1974], which relates the pressure change to a given volume change as

$$E(t) = \frac{1}{C(t)} = \frac{P_v(t)}{V_v(t) - V_o} \tag{2.3}$$

where $E(t)$ is the time varying elastance (mmHg/ml), $P_v(t)$ is the ventricular pressure (mmHg), $V_v(t)$ is the ventricular volume (ml) and V_o is the initial ventricular volume (ml) or the theoretical volume in the ventricle at zero pressure.

To implement the elastance function, the following mathematical representation can be used

$$E(t) = (E_{max} - E_{min})E_n(t_n) + E_{min} \tag{2.4}$$

where E_{min} and E_{max} are constants related to the end-systolic pressure volume relationship (ESPVR) and end-diastolic pressure volume relationship (EDPVR), respectively, and $E_n(t_n)$ is an analytic function normalized between zero and one (in $t_n = 1$), the so-called "double hill" function defined as

$$E_n(t_n) = 1.55 \left[\frac{(\frac{t_n}{0.7})^{1.9}}{1 + (\frac{t_n}{0.7})^{1.9}} \right] \left[\frac{1}{1 + (\frac{t_n}{1.17})^{21.9}} \right] \tag{2.5}$$

where the normalization is calculated by $t_n = \frac{t}{T_{max}}$, $T_{max} = 0.2 + 0.15T_c$ and T_c is the cardiac cycle interval, e.g., $T_c = 60/HR$. The Figure 2.10 shows the elastance function for $E_{max} = 2.0$, $E_{min} = 0.06$, and $HR = 75$ bpm.

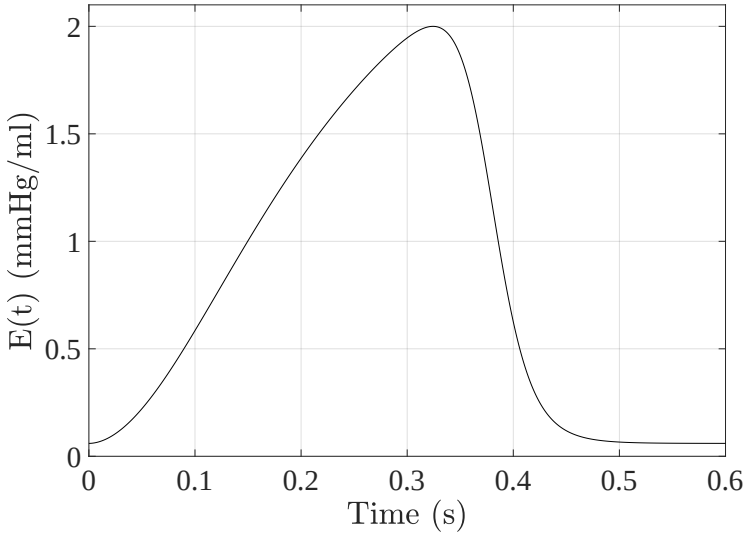

Figure 2.10: Elastance function, $E(t)$, of the left ventricle.

2.2.3 Cardiac Valves Modeling

Heart valves allow the blood to flow in only one direction, so in 0D modeling, they can be represented by a diode in series with a resistance (Figure 2.11). The following equation can calculate the value of blood flow Q that passes through the valve

$$Q = \frac{D(P_1 - P_2)}{R} \tag{2.6}$$

this equation means that if the voltage at point P_1 of the valve is greater than at point P_2, the valve is open, so $D = 1$. Otherwise, if the voltage at point P_1 is less than at point P_2, the valve is closed, so $D = 0$.

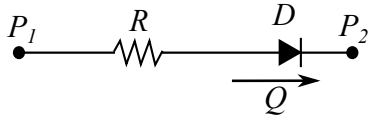

Figure 2.11: The 0D model of a cardiac valve.

The regurgitation phenomenon is a reverse blood flow that occurs when the valves are closed. This phenomenon cannot be represented in the model of Figure 2.11 due to the physical characteristics of the ideal diode. In this work, the regurgitation phenomenon was not considered to simplify the simulations.

2.2.4 0D Modeling of the Left Side of the Heart

Putting all the elements of the left ventricle together as in the Figure 2.12, there is the left atrium (I) as a blood reservoir, then represented by a capacitor; The atrium is directly connected to the mitral valve (II), represented by the resistor and the diode; the left ventricle (III) represented by the variable capacitor; the ventricle is also connected to the aortic valve (IV) and finally the aorta (V) which also behaves as a blood reservoir, therefore represented by a capacitor. Finally, the circuit is connected to the systemic circulation (VI) represented by the Windkessel RLC assembly.

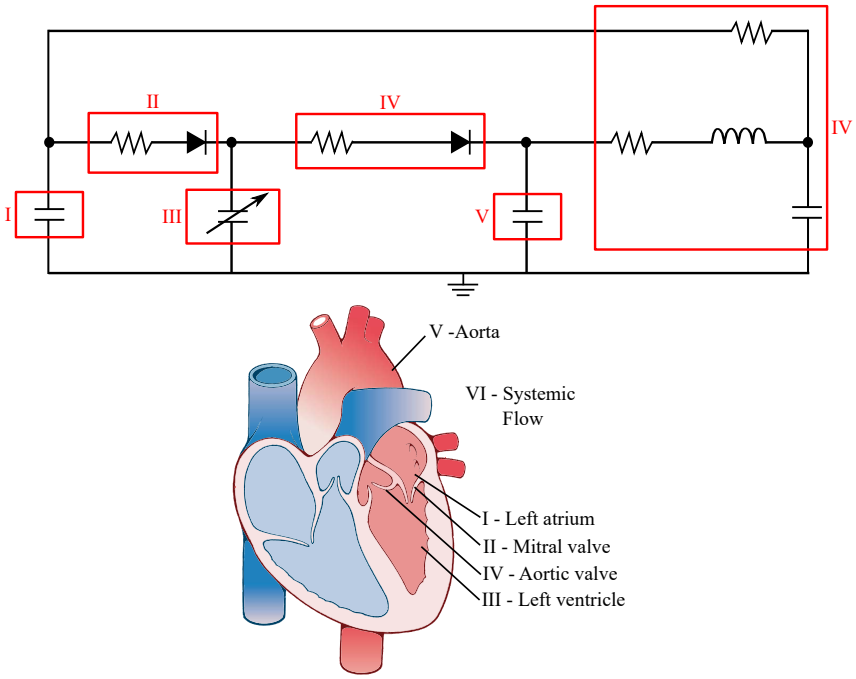

Figure 2.12: Coupling of the left side of the heart in the form of a 0D circuit.

The left ventricular model with the variables and parameters used for calculations is shown in figure 2.13. The original formulation of this model uses the left ventricular pressure, $P_{lv}(t)$, as a state variable. However, this work adapted this model to use the left ventricular volume, $V_{lv}(t)$. This modification was made to avoid using the derivative of time-varying capacitor $C(t)$ to avoid possible numerical instabilities. Using equation (2.3), $P_{lv}(t)$ might be calculated as follows:

$$P_{lv}(t) = E(t)(V_{lv}(t) - V_o). \tag{2.7}$$

Thus, the five state variables of this system without LVAD are: $P_{ao}(t)$, the aortic pressure; $Q_T(t)$, the total flow; $V_{lv}(t)$, the left ventricular volume; $P_s(t)$, the systemic pressure and; $P_{la}(t)$, that is the left atrial pressure. The left atrium is represented by the capacitor C_{la}; the mitral valve is represented by the resistor R_m and diode D_m; and the aortic valve is represented by the resistor R_a and diode D_a and the aortic flow is

Table 2.1: Possible configurations of the valves in the cardiac phases.

State	**Valve**		**Phases**
	Mitral	**Aortic**	
1	Closed	Closed	Isovolumic Relaxation
2	Open	Closed	Filling
1	Closed	Closed	Isovolomic Contraction
3	Closed	Open	Ejection
-	Open	Open	Not feasible

represented by $Q_a(t)$. The behavior of these valves is modeled using ideal diodes taking values of either 1, if valve is open, or 0, if valve is close (see table 2.2.4). The aortic compliance is represented by C_{ao} and the systemic arterial system is modeled using a four-element Windkessel model comprising R_c, L, C_s and R_s.

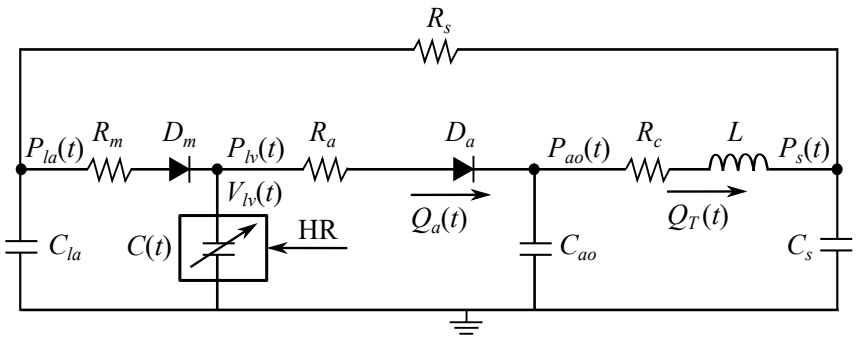

Figure 2.13: 0D model of the left side of the heart.

2.3 Chapter considerations

This chapter introduces the cardiac physiology necessary for understanding the concepts used in this work. The metrics used when analyzing the cardiovascular system were displayed, such as the pressure and volume curves and the pressure-volume loop diagram. In addition, the cardiac cycle was detailed, and the concepts of preload and afterload were described. The chapter also shows how the cardiovascular system is modeled for use in computational calculations.

Then the 0D modeling that uses electrical circuits is detailed. The next chapter will describe ventricular assist devices, such as their function is in the cardiovascular system and how they can be modeled.

Chapter 3

Modeling of the Ventricular Assist Devices

This chapter opens the discussion of Ventricular Assist Devices (VAD). It presents two types of devices, the pulsatile and the rotary. Then, the rotary LVAD 0D modeling is done with an approach similar to the one in chapter 2. The dynamic model of the DC motor controlled by a PI controller is included in the modeling.

3.1 Venticular Assist Devices (VAD)

Cardiovascular diseases are growing at an epidemic rate, and heart transplantation remains the primary treatment for terminally ill patients [Mancini and Colombo, 2015]. However, as the number of patients needing heart transplantation increases, the number of available organs decreases [Ochsner et al., 2014]. Thus, the use of alternative treatments such as Ventricular Assist Devices (VADs) becomes increasingly present [Mancini and Colombo, 2015].

VADs are mechanical devices used to support the blood circulation of patients with heart failure. These devices support the right ventricle (RVAD) or the left ventricle (LVAD) and are used for myocardial recovery, bridge to heart transplantation, or for long-term cardiac treatments [Timms, 2011].

Mechanical circulatory assist devices can be classified according to their outflow as pulsatile or continuous [Timms, 2011].

3.1.1 Pulsatile Ventricular Assist Devices (PVAD)

Pulsatile Ventricular Assist Devices (PVAD) pump blood into the circulatory system through pulses that are pneumatically or electrically generated by diaphragms, bags, or push plates. These devices have a flow characteristic similar to the human heart and are commonly called volume displacement devices [Timms, 2011].

Due to their pulsatile mode of operation, these devices are more likely to present problems with durability and reliability, leading to an increase in the development of rotary ventricular assist devices.

Figure 3.1: A PVAD from [Timms, 2011].

3.1.2 Rotary Ventricular Assist Devices (RVAD)

Rotary Ventricular Assist Devices (RVAD) are operated with continuous flow via a rotating impeller housed within a small pump chamber. The direction to which the blood enters and leaves the impeller determines the type of the RVAD, which can be axial, radial (centrifugal), or mixed flow.

The speed at which the impeller spins depends on the fabricant, but it can vary between 2000 and 15000 rpm to deliver blood flow to the circulatory system. These devices are capable of providing full circulatory support.

Figure 3.2: A RVAD from [Timms, 2011].

3.2 0D Model of Rotary Ventricular Assist Devices

The characteristics of LVADs depend on their manufacture, but all have the purpose of helping the blood flow of patients with cardiac comorbidities. To provide this blood flow, LVADs use certain types of pumps. The most common types of pumps are the centrifugal pump and the axial flow pump.

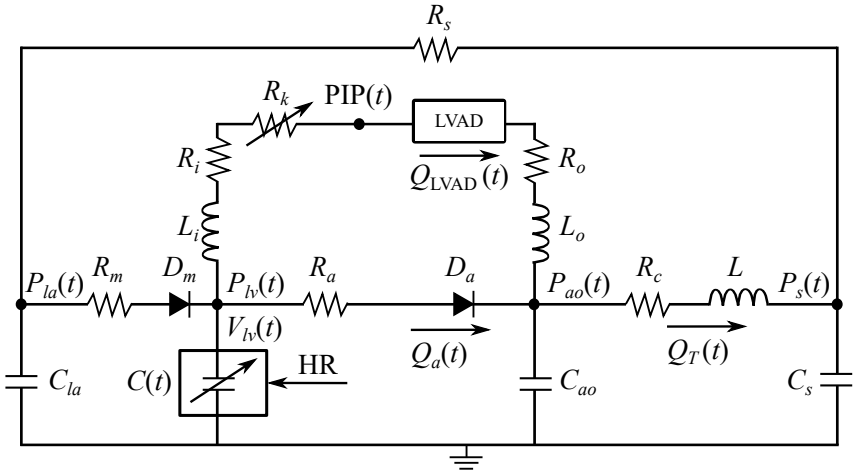

Figure 3.3: 0D model of the left side of the heart with a coupled LVAD.

An LVAD can be coupled to the 0D model as in Figure 3.3. This coupling represents a rotary blood pump described in [Choi et al., 1997]. The coupling of this device to the circuit adds the state, $Q_{\text{LVAD}}(t)$, that represents the blood flow through the LVAD. Resistors R_i and R_o and inductors L_i and L_o represents the inlet and outlet resistances and inertances, respectively. The parameter, R_k, is a time-varying, nonlinear, pressure-dependent resistor that simulates the phenomenon of suction and is described as

$$R_k(t) = \begin{cases} \alpha(P_{lv}(t) - P_{lv-suc}), & P_{lv}(t) \leq P_{lv-suc} \\ 0, & \text{otherwise} \end{cases} \tag{3.1}$$

where α is an LVAD-dependent weight parameter and P_{lv-suc} is a threshold pressure. All parameter values of the CVS-LVAD model and their descriptions are listed in Table 3.1. The pressure difference (inlet-outlet) across the pump, H, is defined by the following equation:

$$H = \beta_0 x_6 + \beta_1 \frac{dx_6}{dt} + \beta_2 \omega^2 \tag{3.2}$$

where ω is the pump speed, and $\beta_0 = -0.17070$, $\beta_1 = -0.02177$ and $\beta_2 = -9.3 \times 10^{-5}$, which are LVAD-dependent parameters.

Table 3.1: CVS-LVAD model parameters

Resistances (mmHg s/ml)		
R_s	1.0000	Systemic vascular resistance
R_c	0.0398	Characteristic resistance
R_m	0.0050	Mitral valve resistance
R_a	0.0010	Aortic valve resistance
R_i	0.0677	Inlet Resistance of Cannulae
R_o	0.0677	Outlet Resistance of Cannulae
R_k	Eq. (4)	Suction Resistance with parameters $\alpha = -3.5$s/ml and $\bar{x}_1$mmHg
Compliances (ml/mmHg)		
$C(t)$	Time varying	Left ventricular Compliance
C_{ae}	4.4000	Left atrial compliance
C_s	1.3300	Systemic compliance
C_{ao}	0.0800	Aortic compliance
Inertances (mmHg s^2/ml)		
L	0.0005	Inertance of blood in aorta
L_i	0.0127	Inlet Inertance of LVAD Cannulae
L_o	0.0127	Outlet Inertance of LVAD Cannulae
LVAD-dependent parameters		
β_0	-0.17070	
β_1	-0.02177	
β_2	-9.3×10^{-5}	

3.2.1 Dynamic model of the LVAD's rotary pump

The simulations results shown in [Simaan et al., 2008] do not take into account the mechanical dynamics of the pump described in [Choi et al., 1997]. It is driven by a brushless DC motor described as:

$$J\frac{d\omega}{dt} = T_e - B\omega - T_p \tag{3.3}$$

where ω is the rotor speed, $J = 0.916 \times 10^{-6}$ is the inertia of the rotor, $B = 0.660 \times 10^{-6}$ is the damping coefficient, T_e is the motor torque. T_p is the load torque on the pump that is dependent of the pump rotor speed and the LVAD flow. This load torque can be defined as:

$$T_p = f(\omega, Q_{\text{LVAD}}) = a_0\omega^3 + a_1\omega^2 Q_{\text{LVAD}} \tag{3.4}$$

where $a_0 = 0.738 \times 10^{-12}$ and $a_1 = 0.198 \times 10^{-10}$ are motor model parameters.

3.2.2 Tunning a PI controller for the LVAD's rotary pump

A PI controller can be tuned to obtain a stable step response and a zero steady-state error; for this consider its closed-loop transfer function to be given by

$$\mathrm{PI}(s) = K_p\left(1 + \frac{1}{T_i s}\right) \tag{3.5}$$

One way of tuning the K_p and T_i parameters is considering the system of the Figure 3.4, if T_p is not taken into account for simplification purposes and the system is in open-loop, then

$$\frac{\omega(s)}{\omega_{\mathrm{des}}(s)} = K_p\left(1 + \frac{1}{T_i s}\right) \times \frac{1}{Js + B} \tag{3.6}$$

after some calculations it can be seen that

$$T(s) = \frac{T_i K_p s + K_p}{T_i s(Js + B)} \tag{3.7}$$

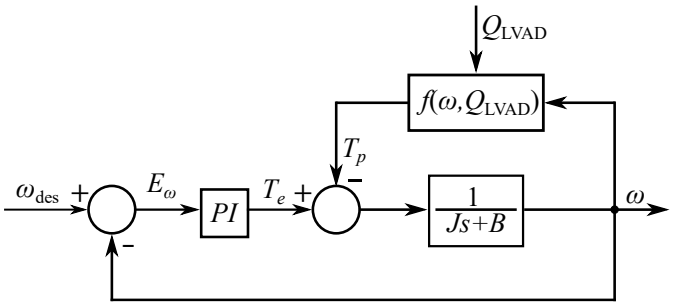

Figure 3.4: Closed loop block diagram for the speed controller.

So to cancel the pole $(Js + B)$ and to obtain a zero steady-state error in the open-loop system, the assumptions are made:

$$K_p = B \tag{3.8}$$

$$T_i = \frac{J}{K_p} = \frac{J}{B}. \tag{3.9}$$

3.3 Cardiac Output Calculation with LVAD

In this work, CO is calculated as the integral of the sum of $Q_{\mathrm{LVAD}}(t)$ and $Q_a(t)$ and this value is kept constant during one cardiac cycle. Let the k-th cardiac cycle beginning at $t = T_c^k$ and ending at $t = T_c^{k+1}$, for $k = 1, 2, \ldots$. The value of CO is only calculated at $t = T_c^{k+1}$, called CO^k, using the values of $Q_{\mathrm{LVAD}}(t)$ and $Q_a(t)$ of the previous cardiac cycle, i.e., from $t = T_c^{k-1}$ to $t = T_c^k$. Hereafter, CO^k is kept constant during the k-th

cardiac cycle, i.e., until $t = T_c^{k+1}$. Discrete and continuous values of CO, CO^k and $\mathrm{CO}(t)$ are defined as:

$$\mathrm{CO}^k = \left[\int_{T_c^{k-1}}^{T_c^k} (Q_{\mathrm{LVAD}}(t) + Q_a(t))\, dt \right] \times \mathrm{HR} \tag{3.10}$$

$$\mathrm{CO}(t) = \mathrm{CO}^k, \text{for } T_c^k \leq t < T_c^{k+1} \tag{3.11}$$

In real clinical situations, $\mathrm{CO}(t)$ can be obtained by estimation strategies [Petrou et al., 2020] or flow sensors.

3.4 Chapter considerations

This chapter introduced ventricular assist devices (VAD), showing pulsatile and rotating devices. Then, the 0D modeling of a rotating LVAD was made, including the dynamic model of the pump, so that the simulation is closer to reality.

The next chapter will present a control strategy for rotary LVAD velocity using systolic pressure and cardiac output as the main parameters.

Chapter 4

Variable Gain SP controller

This chapter describe the SP controller with constant gain and the proposed strategy with the Variable Gain SP controller, emphasizing the limitation without using the controller with gain variation.

4.1 Control Systems applied to rotary VADs

Figure 4.1 shows how VAD control is usually done. The cardiovascular system model (CVS-model) provides one or more hemodynamic variables that are compared with a previously defined reference signal. The error signal $e(t)$ generated by the difference between these signals will serve as input to the controller to determine the device's speed $w(t)$. The device's speed determines the flow of the pump to move blood through the system. The CVS model can also provide hemodynamic variables to modify the VAD velocity as the VAD is coupled to the system.

What differentiates VAD controllers in the literature is the strategy used to modify the speed $w(t)$. Some controllers use classical or modern control theory, and others use computational algorithms or state machines. The objective of the VAD will usually influence which control strategy will be used.

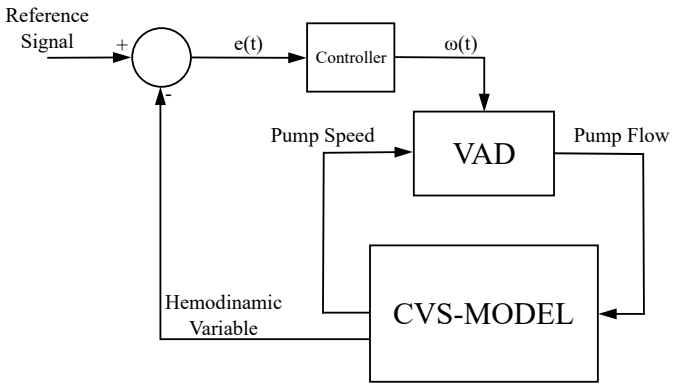

Figure 4.1: Average block diagram for LVAD control.

4.2 Systolic Pressure Controller

Petrou *et al.* developed a control strategy called SP controller that uses the pump inlet pressure (PIP) to calculate the maximum systolic pressure (SP), which is detected within a fixed time interval of 2 seconds to ensure that SP value is detected even for low heart rates [Petrou et al., 2016]. Using Kirchoff's Law, the PIP(t) value is given the equation 4.1.

$$PIP(t) = P_{lv}(t) - L_i\dot{Q}_{LVAD}(t) - R_iQ_{LVAD}(t) \tag{4.1}$$

where $P_{lv}(t)$ is the left ventricular pressure, L_i is the Inlet Inertance of LVAD Cannulae, $Q_{LVAD}(t)$ is LVAD flow and R_i is the Inlet Resistance of Cannulae. The SP value is used to update the pump speed (ω_{des}) according to

$$\omega_{\text{des}} = k_{\text{SP}}(\text{SP} - \text{SP}_{\text{ref}}) + \omega_{\text{ref}} \tag{4.2}$$

where k_{SP} (rpm/mm Hg) is a proportional gain. The values of SP_{ref} (mm Hg) and ω_{ref} (rpm) are reference values obtained during a calibration process, which is done in a simulation environment to identify the pump speed that keeps the desired CO at rest. The value of k_{SP} and the pump speed are adjusted until the desired CO value is obtained. The rotation speed and the systolic pressure value that satisfy the target CO are the values of SP_{ref} and ω_{ref}, respectively, of the equation (4.2).

The performance of the SP controller was evaluated considering changes in preload, afterload, and ventricular contractility (VC). The variables end-diastolic pressure (EDP), CO, and SP were observed and compared with reference values previously defined by a physiological response. The results have shown that the behavior of these variables using the SP controller is better than using constant speed. However, the values were not the same as the physiological reference values. The hypothesis proposed by this work's author is that this fact occurs because of the constant gain k_{SP}. Moreover, the changes in preload, afterload, and VC were tested separately, but these changes can co-occur simultaneously.

4.2.1 Systolic Pressure estimation by peak detection

As the peak pressure values of PIP give the systolic pressure (SP), then a peak detection algorithm is required to obtain the SP value used in the equation 4.2.

The pressure graph is composed of curves with positive and negative peaks. One way of detecting positive peaks is to analyze the moments when the curve reaches its maximum positive values. In this work, the moment in which the second derivative of PIP changes its sign from positive to negative was used, indicating that the curve went from increasing to decreasing so that a local maximum was detected. This peak value is maintained until the subsequent detection. This procedure is summarized in Algorithm 1.

Algorithm 1 SP calculation by peak detection algorithm

Input: PIP^{k-1}, $d\text{PIP}^{k-1}$, P_{ve}^{k}, L_i, $\dot{Q}_{\text{LVAD}}^{k}$, R_i, Q_{LVAD}^{k}

1: $\text{PIP}^{k} = P_{ve}^{k} - L_i\dot{Q}_{\text{LVAD}}^{k} - R_iQ_{\text{LVAD}}^{k}$
2: $d\text{PIP}^{k} = (\text{PIP}^{k} - \text{PIP}^{k-1})/h$
3: **if** ($d\text{PIP}^{k-1} \geq 0$ and $d\text{PIP}^{k} < 0$) **then**
4: $\quad \text{SP}^{k} = \text{PIP}^{k}$
5: **else**
6: $\quad \text{SP}^{k} = \text{SP}^{k}$
7: **end if**
8: **return** SP^{k}

4.3 The Variable Gain SP Controller

The SP controller works well when calibrated for a certain afterload or preload; however, the controller has steady-state error for situations other than calibration. The Equation 4.2 has three constant values, i.e, SP_{ref}, ω_{ref} and k_{SP}. Of these three values, the gain k_{SP} can be changed as a fine adjustment after the calibration process. Therefore, this work suggests the Variable Gain SP Controller, whose equation is given by

$$\omega_{\text{des}} = k_{\text{SP}}(t)(\text{SP} - \text{SP}_{\text{ref}}) + \omega_{\text{ref}}. \tag{4.3}$$

Thus $k_{\text{SP}}(t)$ is a time-varying gain. To elaborate the strategy that will define how $k_{\text{SP}}(t)$ will vary, the physiological cardiac output (CO_{phy}) and the controlled (CO) behavior was used so that $k_{\text{SP}}(t)$ vary as a function of the error (E_{CO}) between these hemodynamic variables.

When E_{CO} is high, $k_{\text{SP}}(t)$ needs to undergo significant changes so that CO approaches CO_{phy}, therefore the growth or decrease of $k_{\text{SP}}(t)$ must be high if E_{CO} is high.

To accelerate the minimization process of this error signal, E_{CO}, positive and negative thresholds, E_{th}^{+} and E_{th}^{-} were empirically defined. If E_{CO} is greater than E_{th}^{+}, it means the k_{SP} value must decrease faster. Thus, its value is updated with a factor that is called of high-threshold Delta (Δ_{high}). However, if E_{CO} is still positive, but smaller than E_{th}^{+}, the k_{SP} value is updated with a factor that is called low-threshold Delta (Δ_{low}). For negative values of E_{CO} the idea is similar, but the k_{SP} should be increased. This logic is described in Algorithm 1. The values of the E_{th}^{+} and E_{th}^{-} and the values of Δ_{high} and Δ_{low} are also empirically defined.

Figure 4.2 shows the block diagram of the variable gain SP controller. The area within the dashed gray line is the dynamic modeling of the rotary pump with a PI controller in a closed-loop. The calculation of CO for updating k_{SP} is done in the area delimited by the black dashed line. The area with gray background is where the SP controller actuates.

Algorithm 2 k_{SP} updating

Input: CO^k_{phy}, CO^k, k_{SP}, Δ_{high}, Δ_{low}, E^+_{th}, E^-_{th}

$E_{\text{CO}} = \text{CO}^k_{\text{phy}} - \text{CO}^k$
if $E_{\text{CO}} > E^+_{th}$ **then**
  $k_{\text{SP}} = k_{\text{SP}} - \Delta_{\text{high}}$
else if $0 < E_{\text{CO}} < E^+_{th}$ **then**
  $k_{\text{SP}} = k_{\text{SP}} - \Delta_{\text{low}}$
else if $E^-_{th} < E_{\text{CO}} < 0$ **then**
  $k_{\text{SP}} = k_{\text{SP}} + \Delta_{\text{low}}$
else if $E_{\text{CO}} < E^-_{th}$ **then**
  $k_{\text{SP}} = k_{\text{SP}} + \Delta_{\text{high}}$
else if $E_{\text{CO}} = 0$ **then**
  $k_{\text{SP}} = k_{\text{SP}}$
end if
return k_{SP}

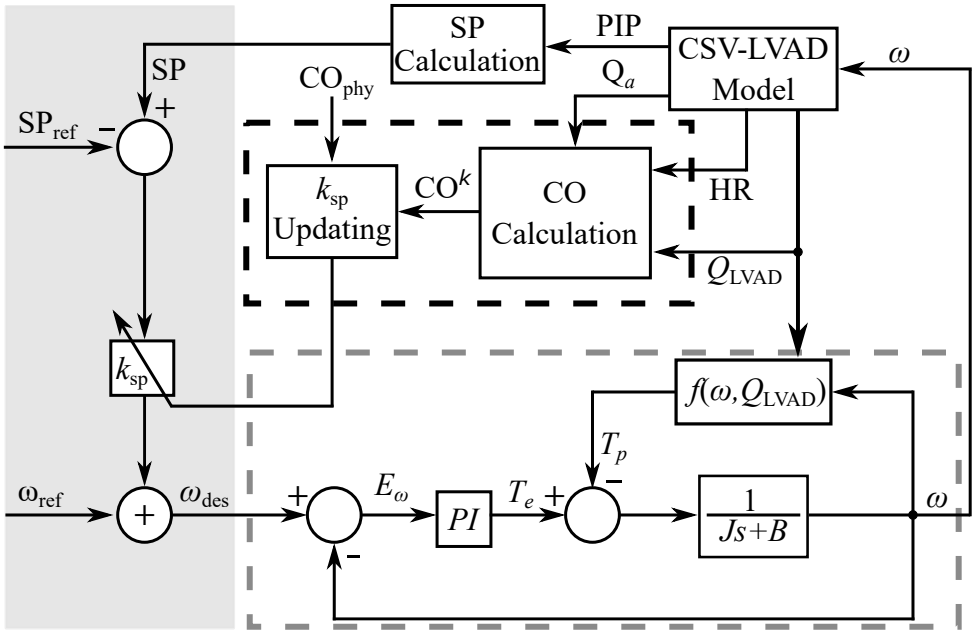

Figure 4.2: Block diagram describing the speed update closed-loop (area within the gray dashed line); the k_{SP} updating (area within the black dashed line); and the control law of the SP controller (area with gray background).

4.4 Chapter considerations

The chapter shows the SP controller among its advantages and the facility to obtain the primary hemodynamic variable to change the LVAD's pump speed when extracting the pressure value at the Pump Inlet Pressure (PIP). However, the SP controller has a constant gain adjusted for a specific preload and afterload value. The controller can not supply the expected cardiac output demand when these hemodynamic values change. For

this reason, the Variable Gain SP controller was proposed, and an algorithm to update the gain was developed and tested.

Chapter 5

Results

This chapter shows the computational simulations for both preload and afterload changes. Simulations are also performed to show how the rotary VAD model implementation works and to show that the closed-loop for the speed controller works as expected with constant or variable rotation speed. Lastly, results shows that the Variable Gain SP controller does have good adaptability under variations in preload and afterload.

5.1 Preload and Afterload Simulation

Performing simulations with varying preload and afterload means changing the patient's physiological condition to test the robustness of some control system applied to LVADs. One way to perform these variations was done in Simaan *et al.* and consists in change the value of the resistance of the Mitral valve R_m for the preload; and change the value of the Systemic Vascular Resistance (R_s) for the afterload [Simaan et al., 2008].

Pressure-Volume (PV) loops, as shown in Figure 5.1, can be used to analyze the effect of changes in both preload and afterload. Changing the value of R_m while keeping constant left ventricular parameters such as E_{max}, E_{min}, and V_0, it is possible to observe the effect in the PV loop and the linear end-systolic pressure-volume relationship (ESPVR). In Figure 5.2 it is illustrated the effect on the PV loop with changes in afterload by varying the value of R_s.

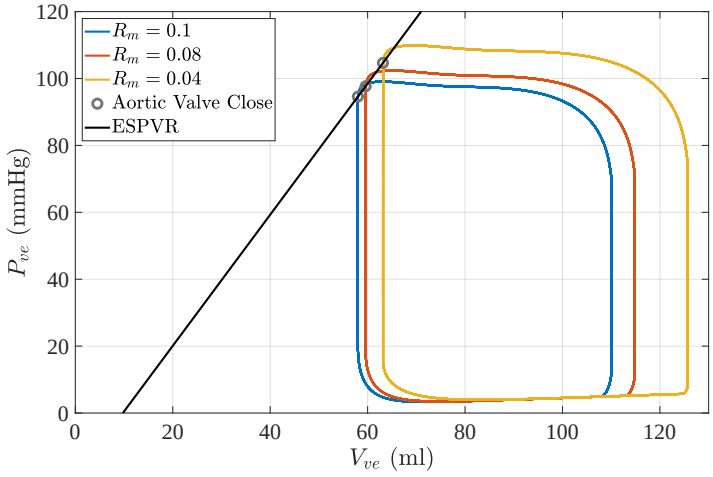

Figure 5.1: PV loops representing preload by changing the mitral valve resistance, R_m.

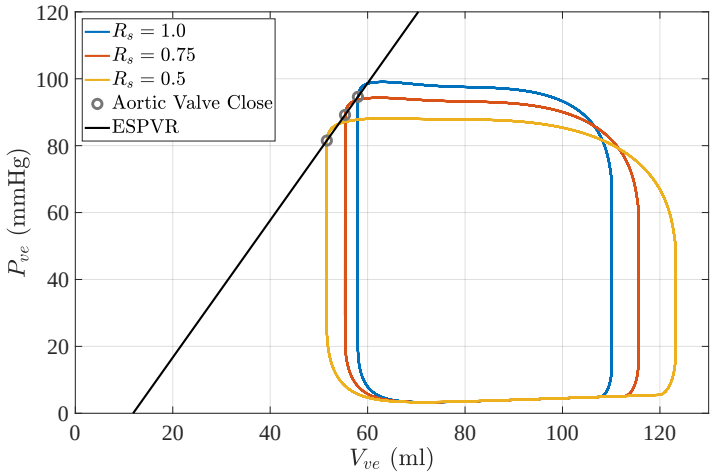

Figure 5.2: PV loops representing afterload by changing the systemic resistance, R_s.

5.2 Simulation results of the LVAD modeling

Figure 5.3 shows the result of a rotary pump simulation with the projected PI in section 3.2.2. As the objective speed was 1000 rpm, the result shows that the pump has zero steady-state error. The controller design using this method has been tested and satisfies the values obtained in [Choi et al., 1997].

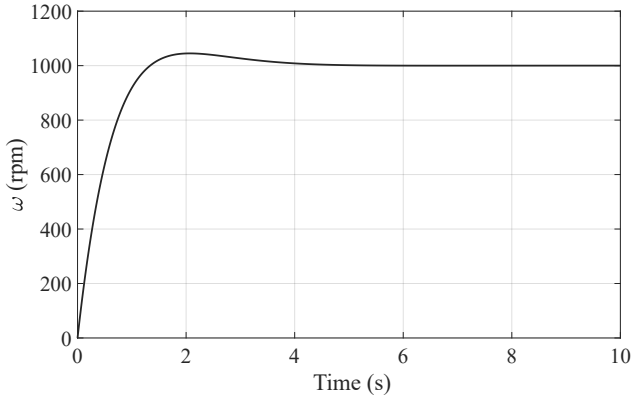

Figure 5.3: Step response of the brushless DC motor.

Figure 5.4 shows the result of a 60-second simulation of the human cardiovascular system model with LVAD at a constant velocity of 9000 rotations per minute. The graph makes it possible to see the pump flow alternating between 6 ml/s and 175 ml/s.

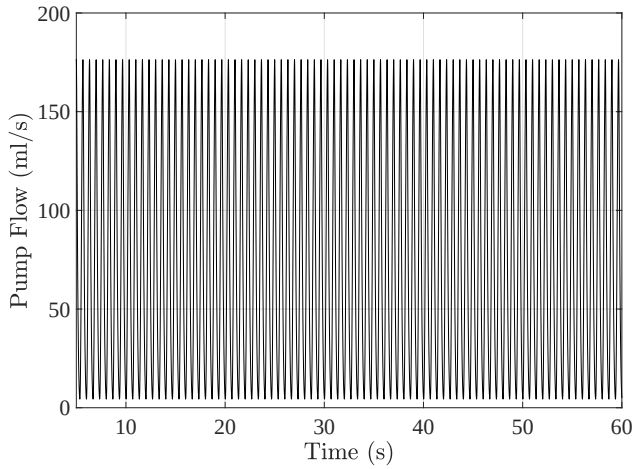

Figure 5.4: Pump Flow signal from human cardiovascular model with constant pump speed of 9000 rpm.

Figure 5.5 shows the result of a 60-second simulation of the CVS-LVAD model with the pump speed increasing linearly from 12000 rpm to 18000 rpm. In the figure, it is possible to see the pump flow as a function of the pump speed. Around 15500 rpm, the phenomenon of suction occurs. The suction is a life-threatening event that damages the walls of the cardiovascular system and should be avoided.

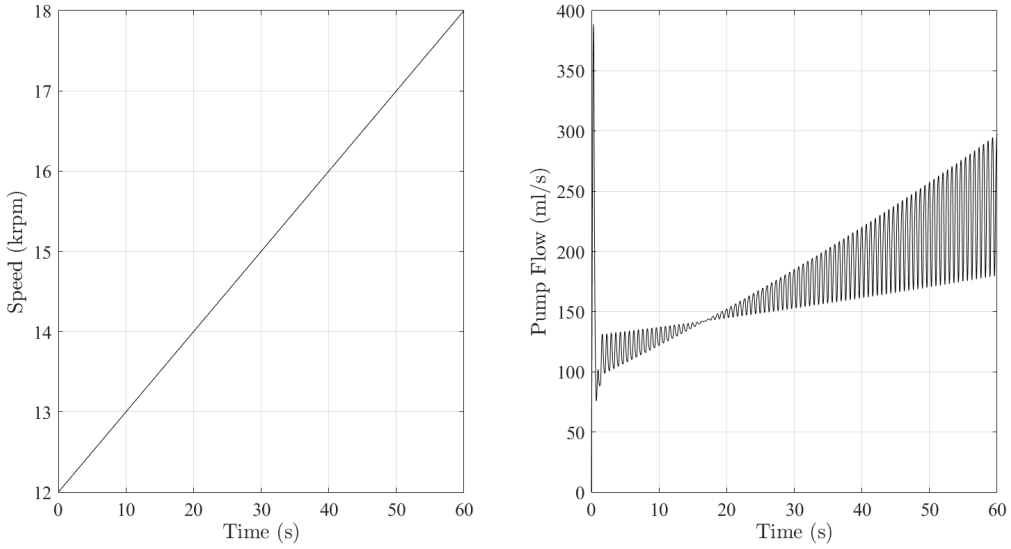

Figure 5.5: Pump Flow signal from human cardiovascular model with pump speed increasing linearly from 12000 rpm to 18000 rpm. Suction phenomenon occurs at 15500 rpm.

5.3 SP Controller Simulation

Figure 5.6 shows the simulation of the pump inlet pressure (PIP), a state variable needed to extract the systolic pressure.

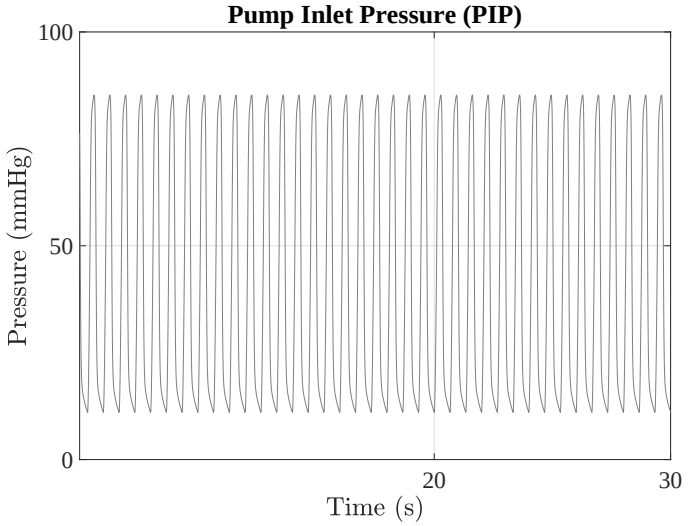

Figure 5.6: Simulation result of the Pump Inlet Pressure (PIP) state variable.

The SP controller responds to changes of preload and afterload in the cardiovascular system; these phenomena can also be visualized through the graph of pressure over time.

Figure 5.7 shows a pressure increase when decreasing the preload through Rm value from 0.1 to 0.05.

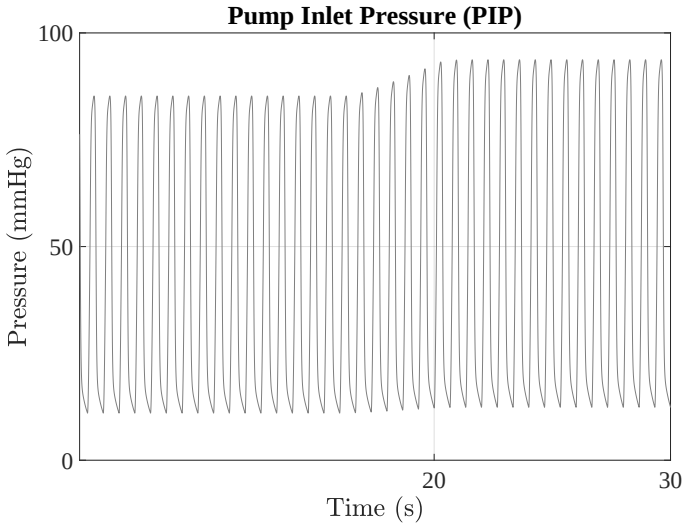

Figure 5.7: Preload increase effect on PIP.

The effect of increasing Rm from 0.1 to 0.5 can be seen in Figure 5.8, where there is a decrease in pressure.

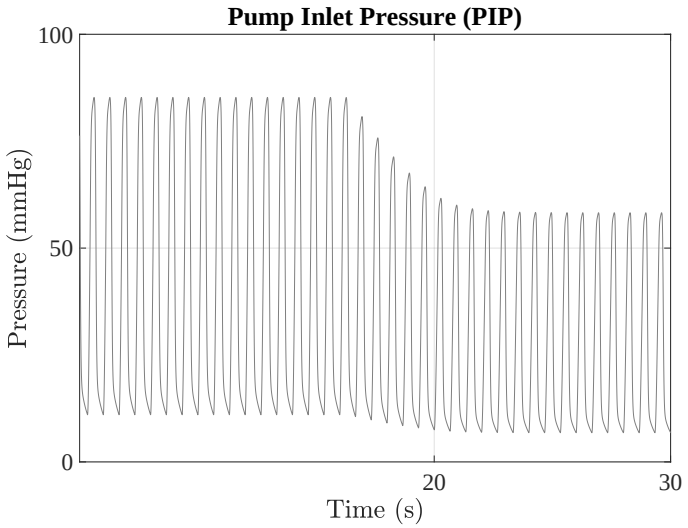

Figure 5.8: Preload decrease effect on PIP.

Similarly, the afterload can be observed in the PIP graph when changing the value of R_s from 1 to 1.5. The result is seen in the Figure 5.9.

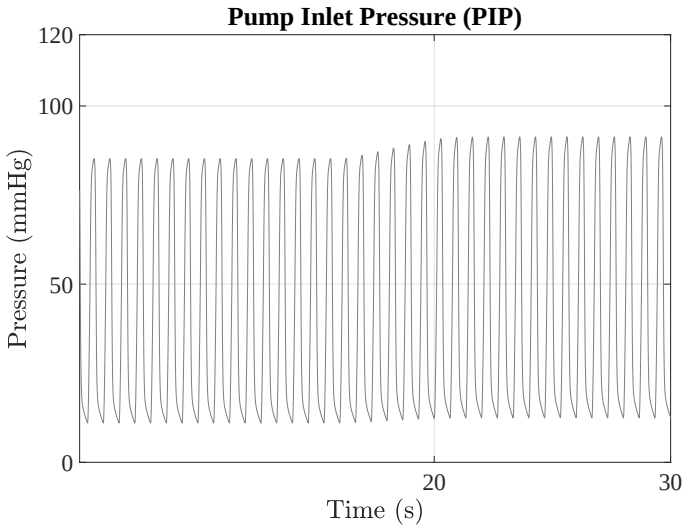

Figure 5.9: Afterload increase effect on PIP.

Decreasing the value of R_s from 1 to 0.5 causes the afterload decrease, as shown in the simulated result of the figure 5.10.

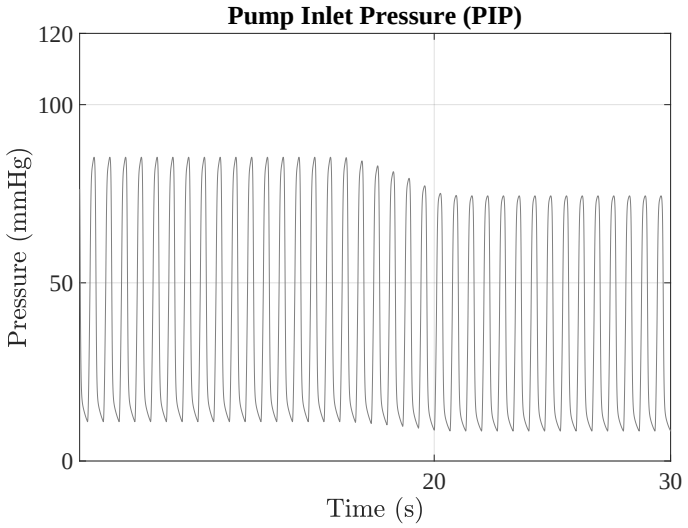

Figure 5.10: Afterload decrease effect on PIP.

A combination of preload and afterload is also possible by changing the value of R_m and R_s (Figure 5.11), and the 120-second simulation result can be seen in Figure 5.12.

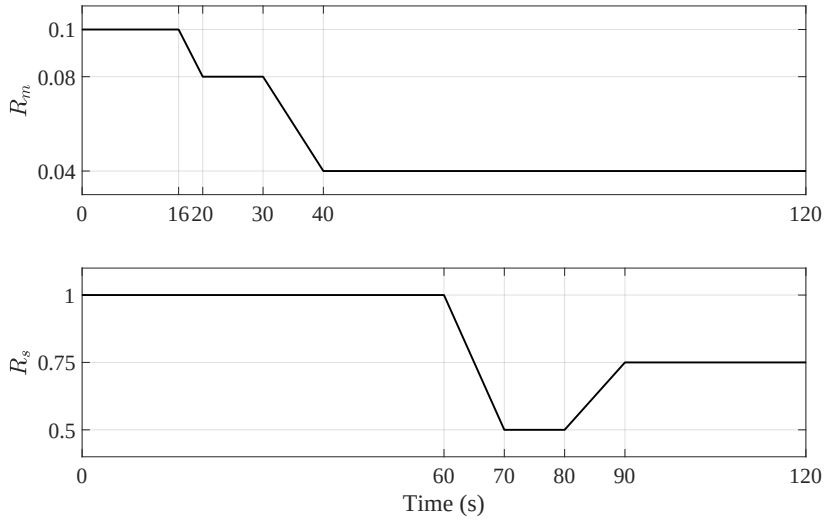

Figure 5.11: Preload and Afterload variation through R_m and R_s.

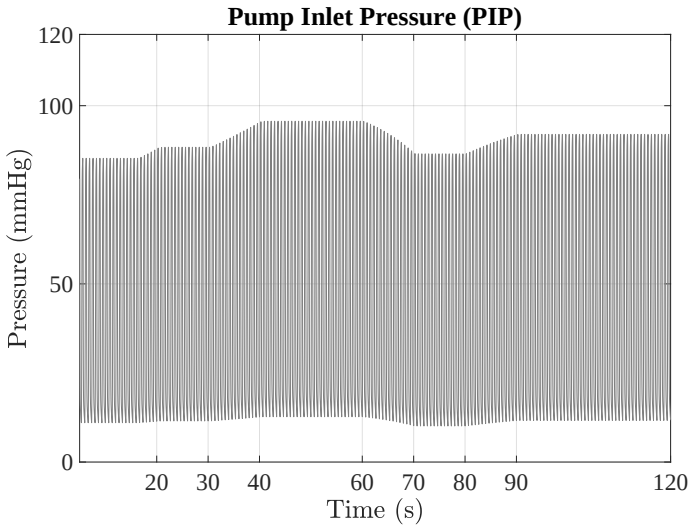

Figure 5.12: Preload and Afterload simultaneously on PIP.

The detection result using the Algorithm 1, proposed in this dissertation, can be seen in Figure 5.13.

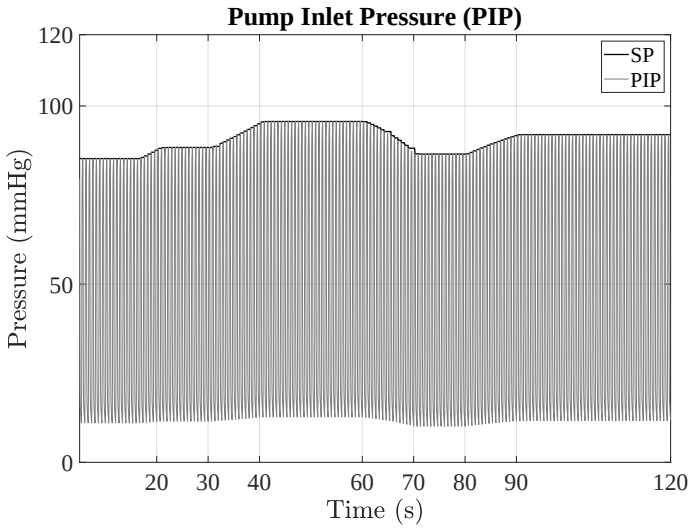

Figure 5.13: Systolic Pressure (SP) value extracted from PIP using the peak detection algorithm.

5.4 Cardiac Output simulation with SP Controller

The SP controller is designed to adapt to preload or afterload exclusively in the simulation from 10 to 25 seconds shown in Figure 5.14 shows an SP controller designed to have a cardiac output next to 4L and preload with $R_m = 0.08$. Initially the simulation starts with the preload of $R_m = 0.1$, then between 16 and 20 seconds the preload varies to $R_m = 0.08$. In the cardiac output graph, the adaptation of the controlled cardiac output (CO) is seen getting closer to the previously defined reference (CO_{phy}). It can be seen from the figure that initially, the controller has a steady-state error when the preload is with $R_m = 0.1$, which is expected since the controller was configured for a preload of $R_m = 0.08$.

The SP controller configured for a afterload with $R_s = 0.5$ has the simulation result shown in Figure 5.15. In this case, as the controller was designed for afterload with $R_s = 0.5$ the controlled CO is able to follow the reference well (CO_{phy}), but When changing the afterload value with $R_s = 0.75$ the controller presents steady state error.

The steady state errors presented in both simulations of Figures 5.14 and 5.15 happen due to the constant parameters of the Equation 4.2 (SP_{ref}, ω_{ref} and k_{SP}), so a new control technique with k_{SP} variable is presented in the next section.

The same behavior of Figures 5.14 and 5.15 can be observed *in vitro* tests in the literature [Petrou et al., 2016].

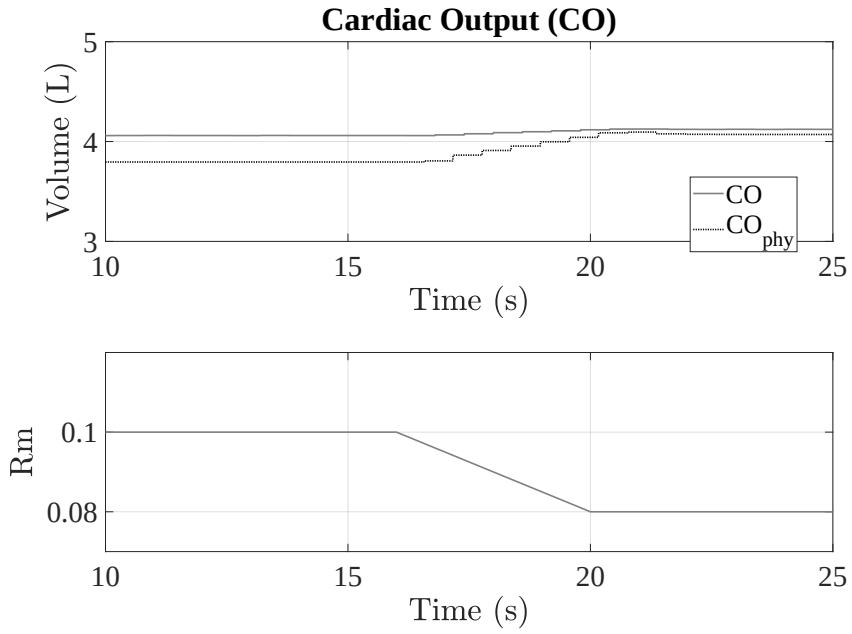

Figure 5.14: Cardiac Output of the SP Controller with preload variation.

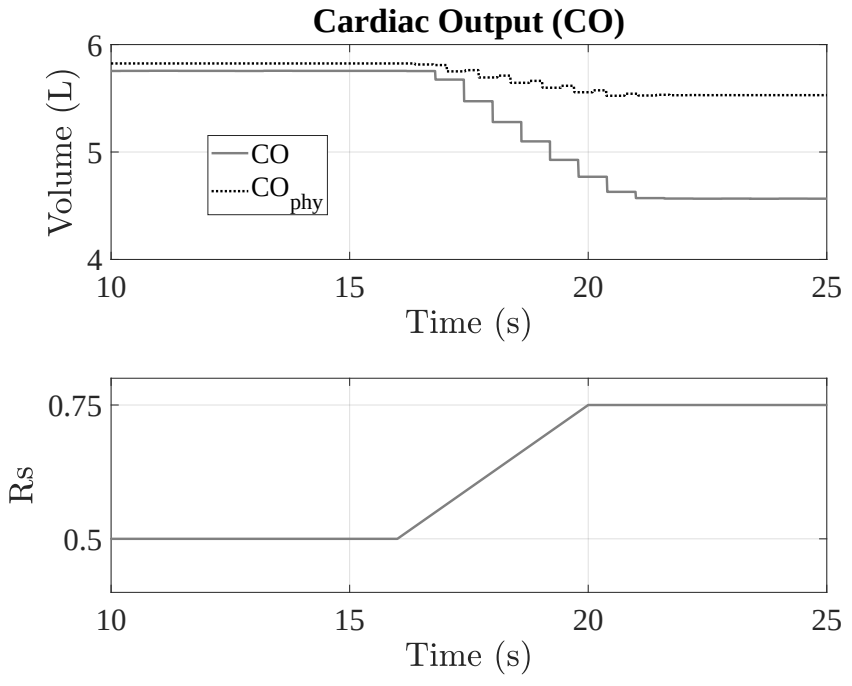

Figure 5.15: Cardiac Output of the SP Controller with afterload.

5.5 Simulations results with Variable Gain SP Controller

To test the performance of the SP controller with variable, calibration was done for a default preload with $R_m = 0.1$. The exact calibration was done for the SP controller with fixed gain, and then both controllers were compared.

In SP controller simulations [Daners et al., 2017], the curves of hemodynamic variables are used as comparison parameters, so this section will show the simulation results for the cardiac output versus time.

In the simulation shown in Figure 5.16 the preload starts with $R_m = 0.1$ and varies to 0.08 in the range of 16 to 20 seconds. As expected, the fixed-gain SP controller experiences steady-state error when the system assumes a preload that it was not designed for.

On the other hand, the variable gain controller has its cardiac output closer to the physiological reference. In Figure 5.16 it is possible to see Algorithm 2 working because when the error between the physiological and the controlled cardiac output is greater, the controller follows the reference more quickly, in the middle of the simulation, when the error is smaller, the controller signal approaches the reference more slowly.

Table 5.5 shows that both the Mean Squared Error (MSE) and the Root Mean Squared Error (RMSE) of the variable-gain controller are smaller than those of the fixed-gain controller.

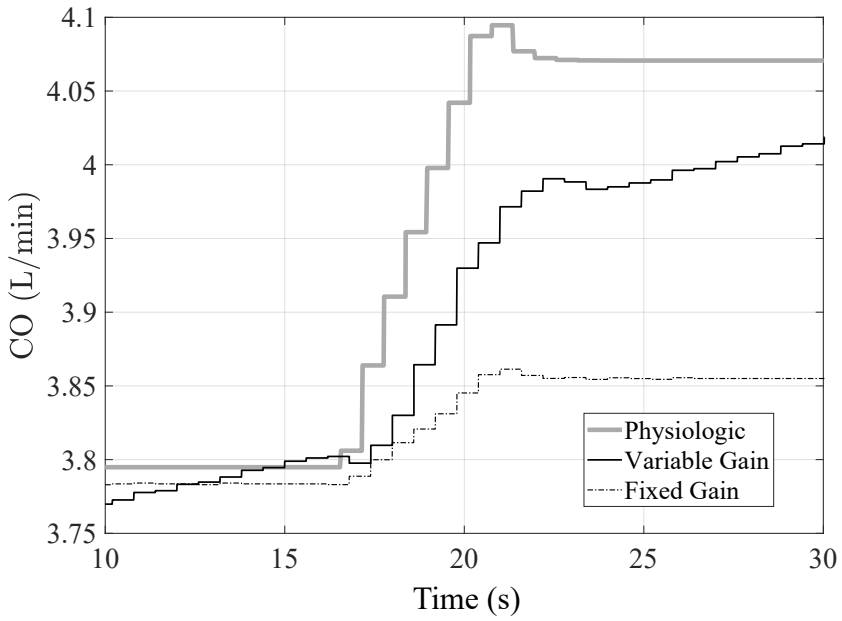

Figure 5.16: Physiologic CO compared with the Variable and Fixed Gain SP Controllers. Increased preload from 10s to 30s of simulation.

Table 5.1: MSE and RMSE compared with Physiologic CO. Increased preload from 10s to 30s of simulation.

SP Controller		
Measure	**Variable Gain**	**Fixed Gain**
MSE	0.0054	0.0266
RMSE	0.0732	0.1631

Figure 5.5 shows another moment of the simulation where the afterload varies from $R_s = 1$ to $R_s = 0.5$. In this simulation, the controller with a variable gain was able to approach the Physiologic CO more quickly and minimize steady-state error. The afterload variation also influenced the controller's behavior with fixed gain. However, this one continues with greater error in steady-state, but as this controller was designed to operate with a pre-set preload and afterload, this result was already expected. The table 5.5 shows the MSE and RMSE obtained in this simulation time.

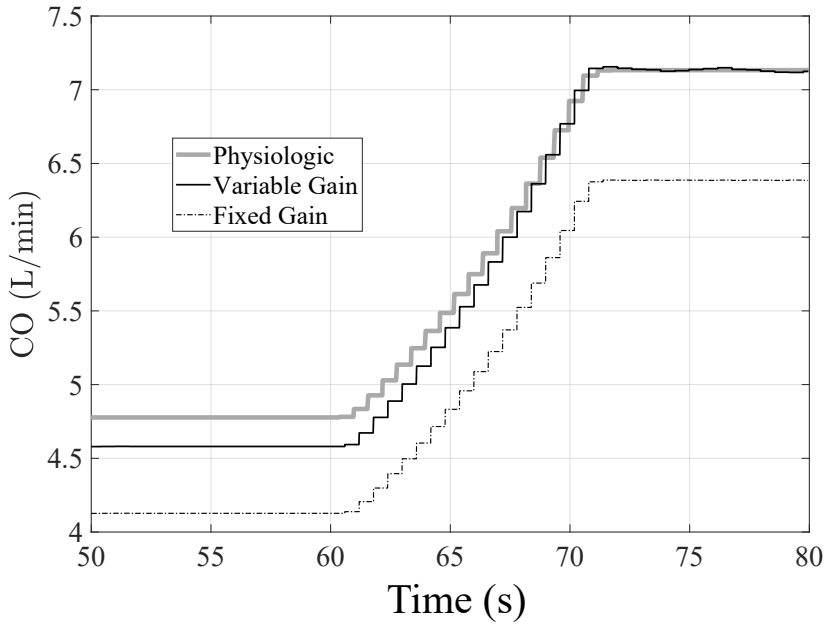

Figure 5.17: Physiologic CO compared with the Variable and Fixed Gain SP Controllers. Increased preload from 50s to 80s of simulation.

Table 5.2: MSE and RMSE compared with Physiologic CO. Increased preload from 50s to 80s of simulation.

SP Controller		
Measure	**Variable Gain**	**Fixed Gain**
MSE	0.0219	0.4923
RMSE	0.1481	0.7016

In the simulation interval shown in Figure 5.18 the afterload value was changed from $R_s = 0.5$ to $R_s = 0.75$ in the interval between 80 and 90 seconds. The controller with a variable gain was able to adapt to this afterload variation in CO and maintained a lower error in the steady-state than the controller with fixed gain. The table 5.5 shows the MSE and RMSE obtained in this simulation time, where the controller values with variable gain are smaller.

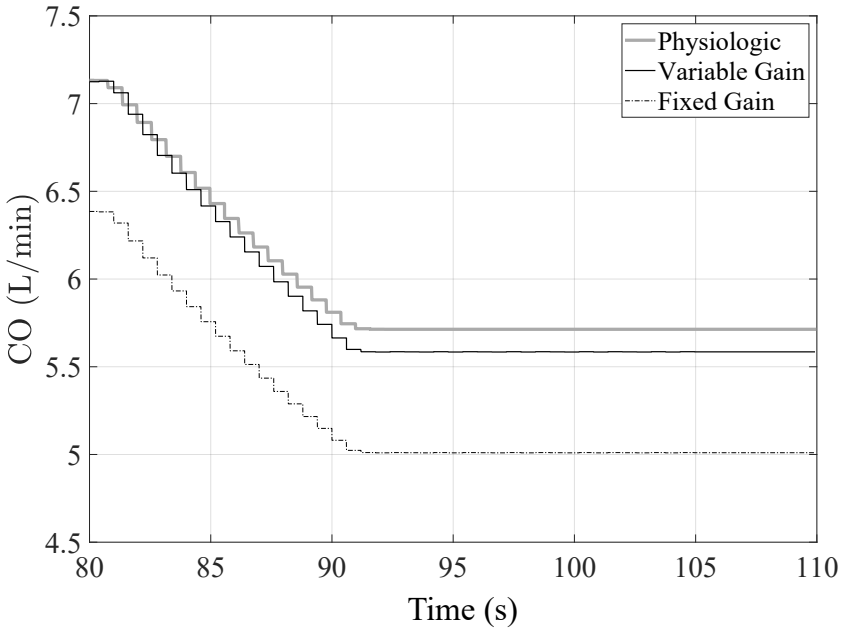

Figure 5.18: Physiologic CO compared with the Variable and Fixed Gain SP Controllers. Decreased afterload from 80s to 110s of simulation.

Table 5.3: MSE and RMSE compared with Physiologic CO. Decreased afterload from 80s to 110s of simulation.

SP Controller		
Measure	**Variable Gain**	**Fixed Gain**
MSE	0.0132	0.5061
RMSE	0.1150	0.7114

The complete simulation is shown in Figure 5.19. The variable gain controller was able to reduce the steady-state error of CO both in the presence of preload and afterload compared to the fixed gain controller.

This result shows that the SP controller, which can adapt the gain k_{SP} according to the expected CO, can obtain better results than the controller with fixed gain. These results were published in the proceedings of the 43rd Annual International Conference of the IEEE Engineering in Medicine and Biology Society [Silva et al., 2021].

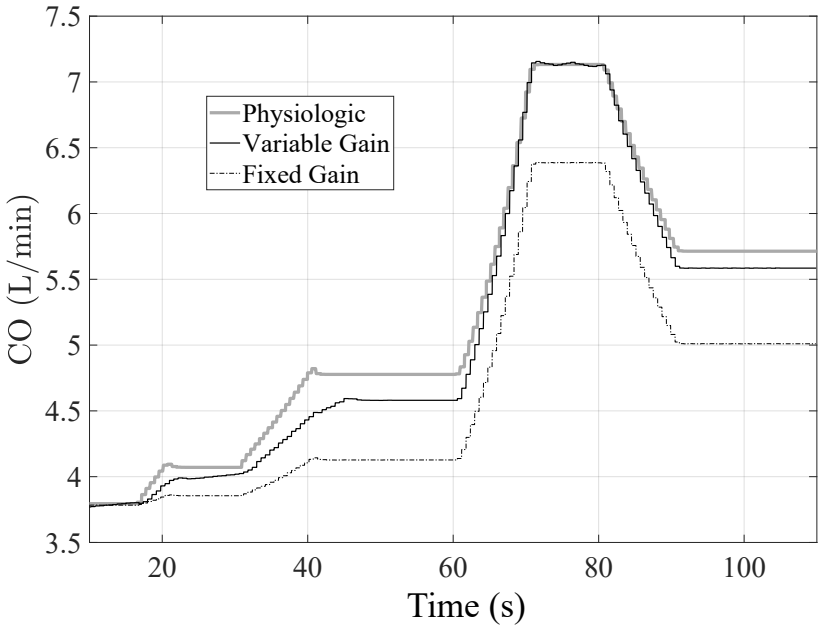

Figure 5.19: Physiologic CO compared with the Variable and Fixed Gain SP Controllers. Preload and afterload variation from 0s to 120s of simulation.

Table 5.4: MSE and RMSE compared with Physiologic CO. Preload and afterload variation from 0s to 120s of simulation.

SP Controller		
Measure	**Variable Gain**	**Fixed Gain**
MSE	0.0216	0.3674
RMSE	0.1469	0.6061

5.5.1 Variable Gain $K_{\mathbf{SP}}(t)$ Analysis

In this subsection, an analysis was made with the gain $K_{\text{SP}}(t)$ of the controller. The experiment consists of CVS-LVAD simulations with a maximum elastance of 1.2 and a minimum of 0.06. The simulations aim to make the system reach a cardiac output of 4.7 L/min, for this the preload and afterload were defined at $R_m = 0.1$ and $R_s = 1$.

It was chosen the values of $K_{\text{SP}}(t)$ equal to 20, 30, 50, 100, 200 and 500. The result can be seen in Figure 5.20, the value of $K_{\text{SP}}(t) = 500$ caused instability in the system, so it was omitted from the figure. The result shows that the smaller the value of $K_{\text{SP}}(t)$, the faster the controller will reach the expected cardiac output and the larger the value of $K_{\text{SP}}(t)$), the slower the controller will be to achieve the same goal.

With $K_{\text{SP}}(t) = 10$ and $K_{\text{SP}}(t) = 20$ it is seen that the controller has reached the cardiac output of 4.4 L/min in parity. However, with $K_{\text{SP}}(t) = 20$ the rise is more linear than with $K_{\text{SP}}(t) = 10$. This happens, because with smaller $K_{\text{SP}}(t)$ more updates are made in the loop of the equation that modifies the LVAD speed.

As a very high $K_{\text{SP}}(t)$ can cause instability in the system or slow down the controller, Algorithm 2 proposes a limiter for the gain $K_{\text{SP}}(t)$. The lower bound of $K_{\text{SP}}(t)$ is set to zero, meaning that the Equation 4.3 will only answer the reference velocity (ω_{ref}).

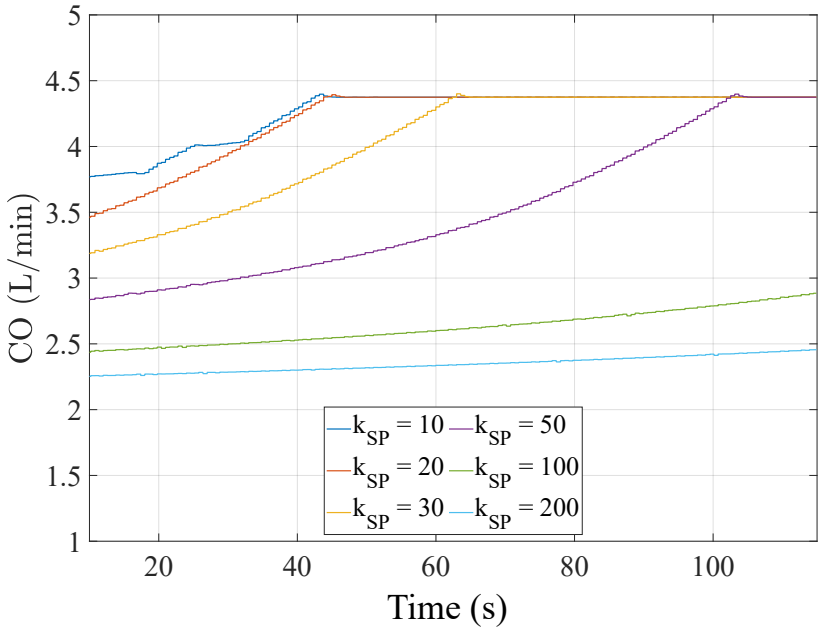

Figure 5.20: Physiologic CO compared with different values of $K_{\mathrm{SP}}(t)$.

The results showed that the Variable Gain SP controller is able to better adapt to preload and afterload variations.

As can be seen, increasing the controller gain leads to slower behavior, which is counter-intuitive when it comes to control theory, e.g., proportional controller. However, this happens because the increase in gain increases the pump speed and the blood flow through the pump. Also, the blood flow in the cardiovascular system is inversely proportional to left-ventricular pressure. Hence, as the controller equation uses systolic pressure, the increase in gain decreases the systolic pressure. This compensation is seen in the sluggishness of the cardiac output response.

Chapter 6

Conclusion

This work presented the implementation of a new controller for left ventricular assist devices (LVAD), the variable gain (VG) systolic pressure controller. The 0D cardiovascular system model, based on the Windkessel model, was used. This model uses electrical circuits to simulate hemodynamic variables through differential equations.

The new variable gain controller presented in this work is an improvement on the fixed gain systolic pressure (SP) controller [Petrou et al., 2016], which was tested using a mock circulatory cardiovascular system. It was used numeric models to reproduce the behavior of the SP controller, representing changes in preload and afterload. As a result, a wide range of different strategies and patient conditions can be tested more efficiently. The mechanical dynamics of the LVAD were also implemented, along with a PI controller designed to calculate the pump speed.

Although the reference value for the cardiac output, CO_{phy}, has been previously defined, it is not necessarily fixed, i.e., its value can be changed any time for experts. Besides, it was proved that the proposed control strategy minimizes the steady-state error in the presence of both preload and afterload changes. This fact did not appear using the SP controller, which operates with a constant gain k_{SP} and was tested either for preload or afterload changes.

6.1 Future works

The SP controller with a constant gain is already well known in the literature with *in vitro* tests. Although the VG controller has presented satisfactory results that indicate the improvement in the performance of the SP controller, these results were made through computational simulations, that is, *in silico*. Implementing the variable gain controller strategy in a hydraulic simulator for research testing is one of the future works.

Another point to be analyzed is the update of the variable gain k_{SP} that can be improved using classical techniques of adaptive control theory or even intelligent techniques. Concerning the values of Δ_{low} and Δ_{high}, other approaches can be evaluated in the future

to improve the convergence of the CO, e.g., fuzzy techniques that are capable of changing the contribution of these Δ's. Furthermore, in real situations, the steady-state error can be relaxed for something around $\pm 5\%$. Ultimately, as future work, the detection of the peaks to calculate SP can be improved, eliminating the use of derivatives.

Bibliography

[AlOmari et al., 2012] AlOmari, A.-H. H., Savkin, A. V., Stevens, M., Mason, D. G., Timms, D. L., Salamonsen, R. F., and Lovell, N. H. (2012). Developments in control systems for rotary left ventricular assist devices for heart failure patients: a review. *Physiological measurement*, 34(1):R1.

[Burattini and Gnudi, 1982] Burattini, R. and Gnudi, G. (1982). Computer identification of models for the arterial tree input impedance: comparison between two new simple models and first experimental results. *Medical and Biological Engineering and Computing*, 20(2):134–144.

[Choi et al., 1997] Choi, S., Boston, J., Thomas, D., and Antaki, J. F. (1997). Modeling and identification of an axial flow blood pump. In *Proceedings of the 1997 American Control Conference (Cat. No. 97CH36041)*, volume 6, pages 3714–3715. IEEE.

[Daners et al., 2017] Daners, M. S., Kaufmann, F., Amacher, R., Ochsner, G., Wilhelm, M. J., Ferrari, A., Mazza, E., Poulikakos, D., Meboldt, M., and Falk, V. (2017). Left ventricular assist devices: challenges toward sustaining long-term patient care. *Annals of biomedical engineering*, 45(8):1836–1851.

[Hall and Hall, 2020] Hall, J. E. and Hall, M. E. (2020). *Guyton and Hall textbook of medical physiology e-Book*. Elsevier Health Sciences.

[King and Lowery, 2017] King, J. and Lowery, D. R. (2017). Physiology, cardiac output.

[Koh et al., 2019] Koh, V. C., Ho, Y. K., Stevens, M. C., Ng, B. C., Salamonsen, R. F., Lovell, N. H., and Lim, E. (2019). A centralized multi-objective model predictive control for a biventricular assist device: An in silico evaluation. *Biomedical Signal Processing and Control*, 49:137–148.

[Malatos, 2016] Malatos, S. (2016). Advances in low-dimensional mathematical modeling of the human cardiovascular system.

[Malchesky, 2017] Malchesky, P. S. (2017). Artificial organs 2016: a year in review. *Artificial Organs*, 41(3):276–304.

[Mancini and Colombo, 2015] Mancini, D. and Colombo, P. C. (2015). Left ventricular assist devices: a rapidly evolving alternative to transplant. *Journal of the American College of Cardiology*, 65(23):2542–2555.

[Ochsner et al., 2014] Ochsner, G., Amacher, R., Wilhelm, M. J., Vandenberghe, S., Tevaearai, H., Plass, A., Amstutz, A., Falk, V., and Schmid Daners, M. (2014). A physiological controller for turbodynamic ventricular assist devices based on a measurement of the left ventricular volume. *Artificial organs*, 38(7):527–538.

[O'Keefe and Singh, 2020] O'Keefe, E. and Singh, P. (2020). Physiology, cardiac preload. *StatPearls [Internet]*.

[Otto, 1899] Otto, F. (1899). Die grundform des arteriellen pulses. *Zeitung fur Biologie*, 37:483–586.

[Petrou et al., 2020] Petrou, A., Kanakis, M., Magkoutas, K., De Vries, B., Meboldt, M., and Schmiddaners, M. (2020). Cardiac output estimation: Online implementation for left ventricular assist device support. *IEEE Transactions on Biomedical Engineering*.

[Petrou et al., 2018] Petrou, A., Lee, J., Dual, S., Ochsner, G., Meboldt, M., and Schmid Daners, M. (2018). Standardized comparison of selected physiological controllers for rotary blood pumps: in vitro study. *Artificial organs*, 42(3):E29–E42.

[Petrou et al., 2017] Petrou, A., Monn, M., Meboldt, M., and Daners, M. S. (2017). A novel multi-objective physiological control system for rotary left ventricular assist devices. *Annals of biomedical engineering*, 45(12):2899–2910.

[Petrou et al., 2016] Petrou, A., Ochsner, G., Amacher, R., Pergantis, P., Rebholz, M., Meboldt, M., and Schmid Daners, M. (2016). A physiological controller for turbodynamic ventricular assist devices based on left ventricular systolic pressure. *Artificial organs*, 40(9):842–855.

[Petukhov et al., 2019] Petukhov, D., Korn, L., Walter, M., and Telyshev, D. (2019). A novel control method for rotary blood pumps as left ventricular assist device utilizing aortic valve state detection. *BioMed Research International*, 2019.

[Silva et al., 2021] Silva, L. F., Cordeiro, T. D., and Lima, A. M. (2021). A variable gain physiological controller for a rotary left ventricular assist device. In *2021 43rd Annual International Conference of the IEEE Engineering in Medicine & Biology Society (EMBC)*, pages 5606–5609. IEEE.

[Simaan et al., 2008] Simaan, M. A., Ferreira, A., Chen, S., Antaki, J. F., and Galati, D. G. (2008). A dynamical state space representation and performance analysis of a

feedback-controlled rotary left ventricular assist device. *IEEE Transactions on Control Systems Technology*, 17(1):15–28.

[Suga and Sagawa, 1974] Suga, H. and Sagawa, K. (1974). Instantaneous pressure-volume relationships and their ratio in the excised, supported canine left ventricle. *Circulation research*, 35(1):117–126.

[Timms, 2011] Timms, D. (2011). A review of clinical ventricular assist devices. *Medical engineering & physics*, 33(9):1041–1047.

[von Platen et al., 2019] von Platen, P., Ruschen, D., Leonhardt, S., and Walter, M. (2019). Assistance ratio: an approach to quantify the hydraulic load distribution in lvad therapy. In *World Congress on Medical Physics and Biomedical Engineering 2018*, pages 745–748. Springer.

[Wang et al., 2012] Wang, Y., Faragallah, G., Divo, E., and Simaan, M. A. (2012). Feedback control of a rotary left ventricular assist device supporting a failing cardiovascular system. In *2012 American Control Conference (ACC)*, pages 1137–1142. IEEE.

[Wetterer, 1940] Wetterer, E. (1940). *Quantitative Beziehungen zwischen Stromstärke und Druck im natürlichen Kreislauf bei zeitlich variabler Elastizität des arteriellen Windkessels; Wetterer, Erik, Dr. med.* JF Lehmanns Verlag.